Medical Oncology (2025) 42:339
https://doi.org/10.1007/s12032-025-02899-8

ORIGINAL PAPER

Green-synthesized silver–copper nanocomposites from *Sargassum latifolium*: antibacterial, anticancer, and in silico pharmacokinetic evaluation

Khaled M. Elattar[1] · Alaa Elmetwalli[2] · Othman R. Alzahrani[3] · Abeer A. Ghoniem[4] · Mervat G. Hassan[5] · Sara Abdelsayed[5] · Ahmed A. Zaher[6] · Deema Kamal Sabir[7] · Ashraf Elsayed[8]

Received: 11 April 2025 / Accepted: 25 June 2025

Abstract

Green synthesis of nanocomposites is an eco-friendly approach compared with conventional methods. *Sargassum latifolium* is a marine microalgae rich in bioactive compounds and represents a promising natural resource for the green synthesis of nanomaterials. This work presents a green protocol for synthesizing, characterizing, and bioactivity of Ag/Cu NC using *Sargassum latifolium* extract. In this context, FTIR analysis showed the involvement of phytochemicals in reducing and stabilizing metal ions. Ag/Cu NC revealed moderate colloidal stability with a zeta potential of − 19.4 mV and an average particle size of 430.0 nm (PDI = 0.408), as evidenced by DLS analysis. EDX and XRD analyses verified a CuO-dominant phase (28.46 wt%) and a crystalline structure containing copper oxide and silver nanoparticles. Although the reduction in phytochemical contents, Ag/Cu NC (IC_{50} = 0.148 ± 1.27 mg/mL), maintained its antioxidant potential compared to *S. latifolium* extract (IC_{50} = 0.108 ± 1.54 mg/mL). Ag/Cu NC revealed privileged antibacterial activity against a series of pathogenic bacterial species, for instance, *B. subtilis* (38.0 ± 1.54 mm) and *S. epidermidis* species (25.0 ± 1.40 mm) as demonstrated by disc diffusion assay. The MIC results established the potential inhibitory of the nanocomposite against *B. subtilis* (0.692 µg/mL). The MTT assays revealed a dose-dependent cytotoxicity of Ag/Cu NCs, with HCT116 cells showing the highest sensitivity (IC_{50} = 8.17 µg/mL), followed by HepG2 cells (IC_{50} = 16.71 µg/mL) and WI-38 cells exhibiting the lowest cytotoxicity (IC_{50} = 84.20 µg/mL). ADME toxicity results indicated moderate to high absorption in HepG2 and HCT116 cells, with significant distribution and metabolism observed at 5–10 µg/mL concentrations. WI-38 cells showed low absorption, distribution, and metabolism. Excretion was minimal across all cell lines. These findings suggest that Ag/Cu NCs exhibit selective cytotoxicity in cancer cells, with limited toxicity in normal cells. Our results in this work indicate the high efficiency of Ag/Cu NC as a novel hybrid in combating oxidative stress, and inhibiting the growth of cancer cells. The study presents an efficient nanocomposite with functional properties of nanomaterials integrated with the bioactivity of natural phytochemicals, paving the way for applications in pharmaceutical and environmental fields.

Keywords Ag/Cu nanocomposite · *Sargassum latifolium* · Characterization · Antibacterial · Anti colon and liver cancer

Introduction

Currently, scientific research is dominated by the synthesis and use of nanoparticles, which are widely applied in animal feed and pharmaceutical industries owing to their unique physicochemical properties [1]. Cu NPs exhibited dynamic properties, including antitumor effect, antibacterial, anticancer, antioxidant, dye decolorization, and catalytic degradation action. However, there are problems with the conventional chemical methods used for nanoparticle production, such as long-lasting technical processes and toxic initial chemicals [2]. The chemical compounds are considered carcinogenic and are, therefore, hazardous to human health [3].

Alternatively, green synthesis of nanoparticles has some benefits, such as sound reduction and stabilization of metal ions [4]. Biological synthesis offers many advantages, including less time-consuming, non-hazardous, and inexpensive approach [5]. This method employs plant,

Alaa Elmetwalli and Khaled M. Elattar contributed equally to this work and shared the first authorship.

Extended author information available on the last page of the article

Published online: 16 July 2025

microorganism, and algae extracts that efficiently act as stabilizing, reducing, and capping agents [6, 7]. Cu NPs formation arises due to the redox reaction of Cu ions with the proteins, amino acids, vitamins, and secondary metabolites such as flavonoids, tannins, polyphenols, terpenoids, and polysaccharides of these extracts [8]. As found in previous research, Cu NPs exhibit both antibacterial and antifungal characteristics, showing enhanced efficiency against bacterial species such as *Escherichia coli, Staphylococcus aureus, Klebsiella pneumoniae, Salmonella typhi,* and *Bacillus subtilis*, as well as antifungal effects against strains such as *Candida albicans* and *Aspergillus niger* [9, 10]. The burgeoning threat of antimicrobial resistance (AMR) has become a serious health issue worldwide, undermining the efficacy of conventional antibiotics. Green-synthesized nanomaterials, in this case, offer promising alternatives with their unique physicochemical properties and multi-targeting mechanism of action. Recent studies, for instance, green synthesis of silver nanoparticles from *Kalanchoe fedtschenkoi* extract, illustrate the efficacy of plant-mediated nanomaterials as effective antimicrobial agents [11].

Furthermore, the results showed that Cu NPs have particular antioxidant activity due to different bioreductive groups on their surface [12]. Thus, concerning the anticancer ability of Cu NPs, their activity has been considered through the generation of ROS, apoptosis, and autophagy mechanisms. They observed that Cu NPs are similarly fatal to cancer cells as normal cells, but the success varied depending on the type of plant extract used [13].

Bimetallic nanoparticles, such as Ag/Cu nanocomposites, have attracted a lot of interest because of their increased physicochemical and biological activity relative to their respective monometallic counterparts. Silver and copper may synergistically respond in a combined nanostructure and thus add more stability, catalytic behavior, and bioactivity to them and making them fantastic possible candidate materials to be used in the fields of therapeutic and antimicrobial possibilities. The Ag/Cu nanocomposites in biopolymer matrices have been reported to exhibit enhanced mechanical, barrier, and antibacterial properties and show good promise for active food packaging applications [14, 15]. Ag/Cu nanocomposites have also exhibited excellent antiplanktonic, antibiofilm, and anti-quorum sensing activities against drug-resistant strains of bacteria [16]. From the materials science perspective, molecular dynamics simulations have confirmed that Ag–Cu systems are dynamically stabilized and structurally stable to degradation upon ion-beam processing in line with their stability and compatibility with advanced applications [17]. In addition, immobilization of Ag/Cu nanoparticles on graphene oxide surfaces or in nanocomposite thin films has been reported to produce highly effective antibiofilm materials [18, 19]. Comparative biological analyses also indicate that Ag–Cu bimetallic nanoparticles are more effective as antimicrobial agents compared to Ag or Cu nanoparticles individually, particularly against plant pathogens and seed health enhancement [20]. These findings convey the promise of Ag/Cu nanocomposites as more effective substitutes for monometallic nanomaterials across various biomedicine, agriculture, and industry applications.

Metal nanoparticles have also attracted significant attention in cancer studies due to their unique physicochemical characteristics that enable them to be used in therapeutic as well as diagnostic purposes. Multifunctionality is a characteristic of nanoparticles and makes them suitable for complementing existing cancer treatment approaches like photodynamic therapy (PDT), where selenium nanoparticles have been used to increase the inactivation of microbial biofilm and cancer cells by light irradiation [21, 22]. Additionally, metal nanoparticles also play a role in radiation therapy, which has been evidenced by their ability to induce resistance in breast cancer cells to be reversed by modulating gene expression when used with sonodynamic sensitizers [23]. In chemotherapy, gold cluster-encapsulated liposomes have been found to be effective nanocarriers of stimuli-responsive drug delivery [24]. Finally, in hyperthermia-based treatments, poloxamer-coated cobalt ferrite nanoparticles have shown significant anti-proliferative activity against prostate cancer cells [25]. In addition to therapy, nanoparticles have also been discovered to be used in diagnostics, with the optical biosensors based on gold nanoparticles being capable of sensitive biomarker detection of cancer-associated biomarkers such as miR-155 [26]. These examples indicate the growing interest in designing multifunctional nanocomposites, such as Ag/Cu, which have dual antimicrobial and anticancer activity, thereby possessing good potential for combined therapeutic applications in oncology.

On the other hand, extensive studies have been done on marine algae as potential sources of nanoparticle formation. Viable methods involve using algae to synthesize nanoparticles since nanomaterials made this way are cheaper despite offering superior yields to rival methods that can only be scaled up at a slow pace [27]. Medical researchers have been able to design nanoparticles that can deliver drugs, genes, or proteins right to the cancerous cells, reducing damage to the other healthy cells and enhancing the treatment's effectiveness [28]. The first aspect that stands out when considering algae type is its flexibility and the fact that different species of algae are metabolically diverse in many ways. Algae comprise various organic compounds like proteins, enzymes, carbohydrates, vitamins, pigments, polysaccharides, and secondary metabolites. In particular, these compounds can be natural reducers in nanoparticle formation [29].

Sargassum sp. belongs to the *phylum Phaeophyta* in the family *Sargassaceae* [30] and inhabits different marine habitats across global continents. Unsurprisingly, this alga

has relatively high sterols, terpenoids, and phenolics [31]. These studies revealed that some compounds possess different pharmacological effects, such as antioxidant, anticancer, immunome, osteogenic, hypoglycemic, anticoagulant, and antimicrobial effects [32]. It was developed by El-Sayed et al. [33] on the biogenesis of silver nanoparticles (Ag NPs) with the brown alga *Sargassum subrepandum*. Further characterization of synthesized Ag NPs showed antibacterial properties against *Fusarium equiseti* and Pseudomonas aeruginosa. Further, other experiments tested the NPs for the cytotoxic effect on the MCF-7 human breast adenocarcinoma cell line with an IC_{50} value of 12.5 µg/mL. In the same manner, Algotiml et al. [34] bio-synthesized Ag NPs by using extracts from different marine algal species, viz., *Ulva rigida*, *Cystoseira myrica*, and *Gracilaria foliifera* acting as reducing as well as capping agents. The cytotoxicity, anticancer, and antimicrobial properties of the Ag NPs were also investigated.

In this study, green synthesis of Ag/Cu NC was carried out using *S. latifolium* extract as a reducer and stabilizing agent. The synthesized nanocomposites were evaluated for their antimicrobial and anticancer properties. Notably, the Ag/Cu NCPs exhibited significant inhibitory effects against *E. coli* and *S. aureus*. In addition, their apoptotic anticancer action against human cervical carcinoma cells was also studied [35]. Due to high surface area and small particle size Ag NPs are highly effective against bacteria like *K. pneumoniae*, *E. coli*, and *S. aureus*; fungi like *C. albicans* and *A. niger*; and viruses such as human immunodeficiency virus and hepatitis B virus [36]. In addition, they have potential as drug delivery agents. They can be applied in chemotherapy and radiotherapy in vitro and animal models of various types of cancer, such as lung cancer, cervical cancer, hepatocellular carcinoma, breast cancer, prostate cancer, and glioblastoma [37, 38].

To the best of our knowledge, this is the first report on the green synthesis of a silver–copper bimetallic nanocomposite using *Sargassum latifolium* as a dual-role reducing and stabilizing agent. Although monometallic Ag or Cu nanoparticles have been prepared from other *Sargassum* species or other marine algae in previous studies, there is no precedent for developing an integrated Ag/Cu nanocomposite through *S. latifolium* and its combined antimicrobial, anticancer, and pharmacokinetic properties remain undetermined. Apart from the bioactivity synergy of the Ag/Cu hybrid in this study, in silico ADME prediction is included to offer prestage insight into its drug-likeness and biomedical utility.

This study aims to (i) investigate the biogenic synthesis of Cu/Ag nanocomposite using the aqueous extract of *Sargassum latifolium*, (ii) characterize the synthesized nanocomposite through UV–Vis spectroscopy, XRD, FTIR, SEM, EDX, zeta potential, and TEM, (iii) evaluate the antioxidant activity, (iv) assess the antibacterial activity against various pathogenic bacterial strains, and (v) explore its potential cytotoxicity effects.

Materials and methods

Reagents

Folin-Ciocalteu reagent (Fluka, Biochemical Inc., Bucharest, Romania), gallic acid (Biomedical Inc., Orange City, FL, USA), 1,1-Diphenyl-2-picrylhydrazyl ($DPPH^{\bullet}$), aluminum chloride, sodium hydroxide, sodium nitrite, catechin, ascorbic acid, and tannic acid were purchased from Sigma-Aldrich (St. Louis, USA). Sodium carbonate was purchased from El-Nasr Pharmaceutical Chemicals (Cairo, Egypt). Silver nitrate ($AgNO_3$) was purchased from *PIOCHEM* for laboratory chemicals (CAS Number: 7761–88-8; purity: 99.5%). Copper sulfate ($CuSO_4$, ≥ 99%) was purchased from EDWIC for Laboratory Chemicals, Egypt.

Instruments

The spectrophotometric analysis, including phytochemical analysis and antioxidant activity, was performed using a Spekol 11 spectrophotometer. Fourier-transform infrared spectroscopy (FTIR) was conducted with a Thermo Fisher Nicolet IS10 Spectrophotometer. Zeta potential measurements were made using a HORIBA Scientific SZ-100 instrument. The nanocomposites' surface morphology, shape, and elemental composition were analyzed using scanning electron microscopy (SEM) with energy-dispersive X-ray spectroscopy (EDX) on an FEI Czech SEM instrument. High-resolution transmission electron microscopy (HR-TEM) was performed with a Thermo Scientific Talos F200i using carbon-coated grids (Type G 200, 3.05 µm diameter, TAAP, USA). X-ray diffraction (XRD) analysis was conducted on a Pan Analytical Philips instrument to assess material properties and crystallographic structure. Additional equipment includes a Beckman Coulter Allegra X-15R Centrifuge and an Elma Schmidbauer GmbH Sonicator.

Preparation of algae extract

Sargassum latifolium was collected from the Red Sea coast near Hurghada, Egypt, and was taxonomically identified by a phycology expert at the Botany Department, Faculty of Science, Mansoura University. The algae materials were washed several times (four times) with distilled water to remove the salts and dried in air at room temperature. *S. latifolium* (10 g) was transferred into a conical flask and mixed with 100 mL of deionized water. The flask containing the mixture was placed in a horizontal water bath shaker at 70 ℃ for 20 min and left to cool at room temperature. The mixture

was soaked overnight at room temperature with occasional stirring and then filtered. The extract was used immediately to prepare nanomaterials and phytochemical and biological assessments. The remained extract was stored in a dark glass vessel at 0–54 ℃ to preserve its quality [39, 40].

Green synthesis of Ag/Cu NC

A solution of silver nitrate (40 mL, 1 mM) was prepared in deionized water. *S. latifolium* extract (60 mL, 5.98 mg/mL) was added dropwise to the $AgNO_3$ solution with continuous stirring at room temperature and heating until 55 ℃ after adding the silver nitrate solution. The solution's deep yellow color turns dark brown after 30 min. A solution of copper sulfate (40 mL, 1 mM) prepared in deionized water was dropwise added to *S. latifolium* extract (60 mL, 5.98 mg/mL) with stirring of the mixture at 70 ℃ until a distinct color change was accomplished (≈ 5 h). A mixture of silver and copper nanoparticle solutions was obtained by mixing both solutions under stirring conditions for 1 h at 60 ℃. The mixture was stirred for 4 h and sonicated for 1 h under heating at 60 ℃ at 60 ℃. To isolate the solid nanoparticles for SEM, EDX, and XRD analyses, the mixtures were centrifuged, and the precipitated solid was washed with ethanol and deionized water and dried at 60 ℃ for 24 h [41].

Phytochemical analysis

The phytochemicals of the algae extract and synthesized nanomaterials were also determined quantitatively using various standard color metrics. Folin-Ciocalteu reagent was employed to investigate the TPC, in which the samples interacted with the reagent to form a blue color complex with color intensity depending on the amount of polyphenol content [42, 43]. Absorbance was measured at $\lambda = 765$ nm, and phenolic content was calculated based on a calibration curve prepared from gallic acid ($y = 0.0062x$, $R^2 = 0.987$), and results were noted in terms of mg of gallic acid equivalent (GAE) / g of dried sample. Quantitative analysis of flavonoids was performed using the aluminum chloride colorimetric assay [44]. The interaction of the samples with aluminum chloride reagent led to the forming a blue color complex to indicate the presence of flavonoids. The samples' absorbance was recorded at $\lambda = 520$ nm, and the results acquired from the catechin standard equation $y = 0.0028$ x, $R^2 = 0.988$, were expressed as milligrams of CE/gram of dry weight. Tannin content (TTC) was analyzed using the vanillin–HCl method [45], where 1 mL of the sample was mixed with 5 mL of freshly prepared vanillin–HCl reagent. The mixture was allowed to react for 20 min at room temperature, and the absorbance was measured at $\lambda = 500$ nm. The tannin content was estimated from the tannic acid standard curve ($y = 0.0009x$; $R^2 = 0.955$) and expressed as a milligram of TAE per gram of the dried sample.

Assessment of antioxidant activity

The free radical scavenging activity of the algae extract and the nanocomposite was determined using the DPPH radical scavenging method, as described earlier by [46], with ascorbic acid as the standard reference. These samples were successfully diluted in methanol, and 0.135 mM DPPH solution was added. The obtained mixtures were incubated in the dark for 30 min before their absorbance values were measured at 517 nm. The remaining DPPH radical percentage was calculated using the formula (Eq. 1):

$$\%\, DPPH\ radical\ remaining = \left([DPPH]^t / [DPPH]^0\right) \times 100 \quad (1)$$

To determine the IC_{50} value, a plot of the remaining DPPH radical percentage against the sample concentration was created, which follows an exponential curve. The IC_{50} value corresponds to the sample concentration that inhibits 50% of the DPPH radicals, with the lower value indicates stronger antioxidant activity.

Microbial susceptibility test

Agar well diffusion method

To ascertain the antibacterial inhibitory activity of the algae extract and the nanocomposite against the pathogenic bacteria, the agar well diffusion method [47] was used. In this method, the inoculum volume on the agar surface was spread over the entire area of the agar plate. Next, an aseptic punch with a 6 to 8 mm diameter was made, following which 100 µm of all the tested samples were placed in the well. After that, the agar plates are incubated under appropriate conditions, depending on the type of test microorganism used. The antimicrobial agent spreads within the agar medium and prevents the growth of the particular microbial strain used for testing.

Minimum inhibitory concentration (MIC)

A microdilution assay assessed the MIC of the most potent antibacterial agents [48]. A control tube was prepared with inoculated broth without adding the nanomaterial sample. A serial dilution of the sample in concentrations ranging from 0.346 to 5670 µg/mL was used to determine MIC in the nutrient broth medium. The control contained only inoculated broth and was incubated for 24 h at 37 ℃. The MIC endpoint is the lowest concentration of the sample in which no visible growth is seen in the tubes. The visual turbidity of the tubes was noted, both before and after incubation, to

confirm the MIC value, and DO was measured at 600 nm to confirm the result.

Anticancer activity evaluation

Cell culture and treatment modifications

Human cell lines WI-38, HCT116, and HepG2 were cultured at 37 ℃ in a humidified incubator with 5% CO_2 in Dulbecco's Modified Eagle Medium (DMEM, Cat# 11,965–092, Thermo Fisher Scientific, Waltham, MA, USA) supplemented with 10% fetal bovine serum (FBS, Cat# 16,001–048, Thermo Fisher Scientific, Waltham, MA, USA) and antibiotics (100 U/mL Penicillin, Cat# 15,149–128, Thermo Fisher Scientific, Waltham, MA, USA; 100 µg/mL Streptomycin, Cat# 16,144–127, Thermo Fisher Scientific, Waltham, MA, USA). For 40–50% of the assays, cells were subcultured when they reached 80–90% confluency. The treatments were administered for 48 h, with morphological evaluations conducted at 24 and 48 h. Drug concentrations were based on half-maximal inhibitory concentrations (IC50/2) [49, 50].

Cell viability assay

The MTT assay (Cat# M6591, Thermo Fisher Scientific, Waltham, MA, USA) assessed cell viability. A549 and WI-38 cells were seeded in 96-well plates (Cat# 3192, Corning, Corning, NY, USA) and exposed to varying concentrations of chitosan (Cat# 348,827, Sigma-Aldrich, St. Louis, MO, USA) and curcumin (Cat# C1386, Sigma-Aldrich, St. Louis, MO, USA) for 48 h. After adding the MTT reagent, formazan crystals were dissolved in dimethyl sulfoxide (DMSO, Cat# D7417, Sigma–Aldrich, St. Louis, MO, USA), and cell viability was determined relative to untreated controls by measuring absorbance at 570 nm using a microplate reader (SpectraMax M5, Molecular Devices, San Jose, CA, USA). IC50 values were calculated using GraphPad Prism software (GraphPad Software, San Diego, CA, USA) [51].

ADME predictions

Computational methods were employed to predict the absorption and distribution characteristics of the compound. The SwissADME tool (available at SwissADME, http://www.swissadme.ch) was used to calculate lipophilicity (LogP), which is crucial for understanding the compound's absorption potential. SwissADME also predicted water solubility, which influences the compound's absorption in the gastrointestinal system and solubility in aqueous environments. Furthermore, SwissADME evaluated the compound's likelihood of gastrointestinal absorption, categorizing it as high, moderate, or low. The program also predicted blood–brain barrier (BBB) permeability, providing insight into the compound's potential to cross the brain. Metabolism and toxicity were forecasted using admetSAR (admetSAR-2.0; available at http://lmmd.ecust.edu.cn/admetsar2), which provided data on the compound's metabolic stability in the liver and potential genotoxicity, indicating its ability to cause genetic mutations [50, 52]. We emphasize that these predictions do not represent actual ADME properties of the entire Ag/Cu nanocomposite, but rather serve to offer hypothesis-generating insights into the behavior of bioactive molecules that may interact with or influence nanoparticle–cell interactions.

Statistical analysis

All experimental data are expressed as mean ± standard deviation (SD) from three independent biological replicates ($n = 3$), each performed in technical triplicates. Statistical analyses were conducted using GraphPad Prism version 9.0 (GraphPad Software, San Diego, CA, USA). For cytotoxicity (MTT) assays, dose–response curves were plotted using non-linear regression (log[agonist] vs. normalized response – variable slope), and IC_{50} values were calculated with 95% confidence intervals. For antibacterial activity (zone of inhibition) and phytochemical comparisons, one-way analysis of variance (ANOVA) was employed to determine statistically significant differences between treatment groups. A p-value of < 0.05 was considered statistically significant. All statistical tests were two-tailed unless otherwise indicated.

Results

Characterization of Ag/Cu NC

UV–Visible spectroscopy

UV–visible (UV–Vis) spectroscopy was employed to study the optical characteristics of the extract of *S. latifolium* and Ag/Cu NC (Fig. 1). UV–Visible spectra of the two samples were obtained to identify absorbance at different wavelengths. The spectrum analysis of *S. latifolium* extract presented a more intense absorption band at 506 nm with an absorbance intensity of 0.974. The Ag/Cu NC UV–Vis spectrum was characterized by a maximum absorption peak recorded at 782 nm with an absorbance of 0.957.

FTIR spectral analysis

In the FTIR profile of *S. latifolium* extract, several characteristic peaks appeared that correspond to different functional groups that may be associated with phytochemical components of the plant (Fig. 2). The broad peak at 3448 cm^{-1}

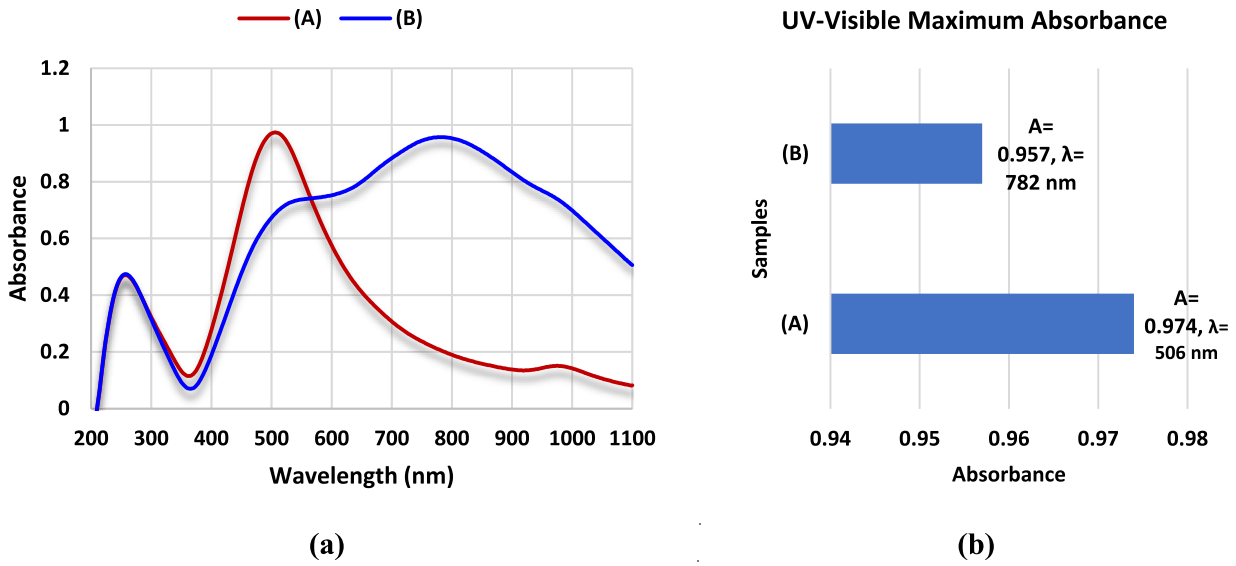

Fig. 1 UV–Visible spectroscopy of *S. latifolium* extract and Ag/Cu NC. **a** Referring to the plotted diagram of absorbance values recorded at different wavelengths (nm). **b** A comparison of the maximum absorption peaks at varied wavelengths. **A** refers to *S. latifolium* extract, and **B** refers to Ag/Cu NC

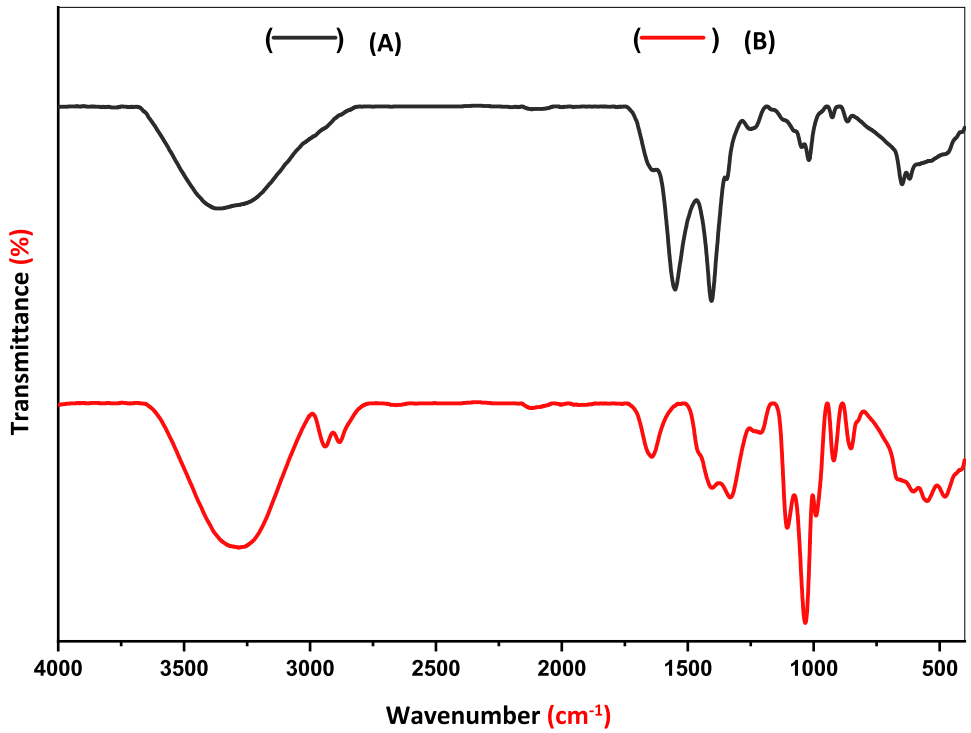

Fig. 2 FTIR spectra of *S. latifolium* extract and Ag/Cu NC. **A** refers to *S. latifolium* extract, and **B** refers to Ag/Cu NC

is attributed to the O–H stretching of phenolic and alcohol of hydroxyl groups. The broad bands around 2950 and 2889 cm^{-1} are attributed to the C–H stretching vibrations of the aliphatic hydrocarbon. The band at 1549 cm^{-1} is attributable to aromatic C = C stretching characteristic of flavonoid and polyphenol content. Further peaks at 1406 and 1342 cm^{-1} relate to C–H bending, and those at 1260 and 1226 cm^{-1} to C–O stretching in ethers and esters. The bands located at 1050 and 1018 cm^{-1} have been assigned to the C–O and C–C in carbohydrates. Other bands at 926, 867, 650, and 619 cm^{-1} are ascribed to functional groups' interaction, contributing to secondary metabolites like tannins and terpenoids. In the FTIR spectrum of the Ag/Cu NC, notable shifts and additional peaks were observed

compared to the *S. latifolium* extract, suggesting the interaction of phytochemical components with the nanoparticles. The O–H stretching band, which appeared at 3448 cm^{-1} in the extract, shifted to 3321 cm^{-1} in the nanocomposite, indicating hydrogen bonding and interaction between hydroxyl groups and metal nanoparticles. The functional groups of aliphatic hydrocarbons were slightly altered in the nanocomposite since the C–H stretching absorption bands of the nanocomposite at 2939 and 2882 cm^{-1} were shifted somewhat compared to the extract. New absorption bands at 1662 and 1641 cm^{-1} appeared in the Ag/Cu NC referred to a carbonyl (C = O) stretching frequency, due to polyphenols or flavonoids involved in reducing silver and copper ions. The shift of the band at 1464 cm^{-1} (aromatic C = C stretching) in the nanocomposite indicates structural alteration of aromatic moiety within the formation of nanoparticles. Other changes include those at 1409, 1324, and 1202 cm^{-1}, confirming phytochemicals and metal nanoparticle interactions. Additional absorption bands new to the nanocomposite, located at 545 and 477 cm^{-1}, can be attributed to the metal–oxygen (M–O) stretching vibrations, indicating the successful synthesis of Ag/Cu NC. The spectral shifts confirm the active participation of phytochemicals from the *S. latifolium* extract in both the bioreduction and stabilization of Ag and Cu nanoparticles, highlighting the integration of plant-derived functional groups into the nanocomposite matrix.

Zeta potential and DLS analysis

In the present study, the zeta potential of Ag/Cu NC was observed at − 19.4 mV (Fig. 3a). The negative value revealed that particles have a negative surface charge, implying that nanoparticles are electrostatically stable in dispersion. A zeta potential value beyond ± 15 mV is generally considered adequate to maintain dispersion stability over time, and thus, the observed value supports the notion that the nanocomposite formulation is suitably stable for biological applications. Also, the mean electrophoretic mobility of the nanocomposites was determined, and its notation of − 0.000150 cm^2/Vs indicated the stability of the dispersion of the nanoparticles because of electrostatic repulsive forces between particles.

The DLS analysis of Ag/Cu NC exhibited an average size of 430 nm and PDI of 0.408, indicating that the sample is moderately polydispersed (Fig. 3b). Polydispersity Index (PDI) values ranging less than 0.5 comparatively suggest that the sample consists of particles of nearly equal size distribution, although there may be a slight difference. It needs to be noted that the hydrodynamic diameter in the DLS measurement includes not just the metallic core but also the accompanying organic molecules or hydration layers, which may be responsible for the observed increase in apparent size. This has been perhaps the reason why particle size was given a different value when using DLS compared to other techniques, such as TEM. Their size range and colloidal stability are of particular interest for their anticipated interaction with biological membranes, in which sub-micron particles were found to enhance cellular uptake and antimicrobial activity.

High-resolution transmission electron microscopy (HR-TEM)

The HR-TEM images revealed a heterogeneous Ag/Cu NC population with various morphologies (Fig. 4). The particles display a range of shapes, including spherical, hexagonal, and truncated hexagonal forms, suggesting that the nanocomposite consists of nanoparticles that undergo different growth mechanisms. The size distribution is broad, with particles varying from a few nanometers to several tens of nanometers in diameter. Additionally, crystalline lattice fringes are visible in some of the nanoparticles, indicating

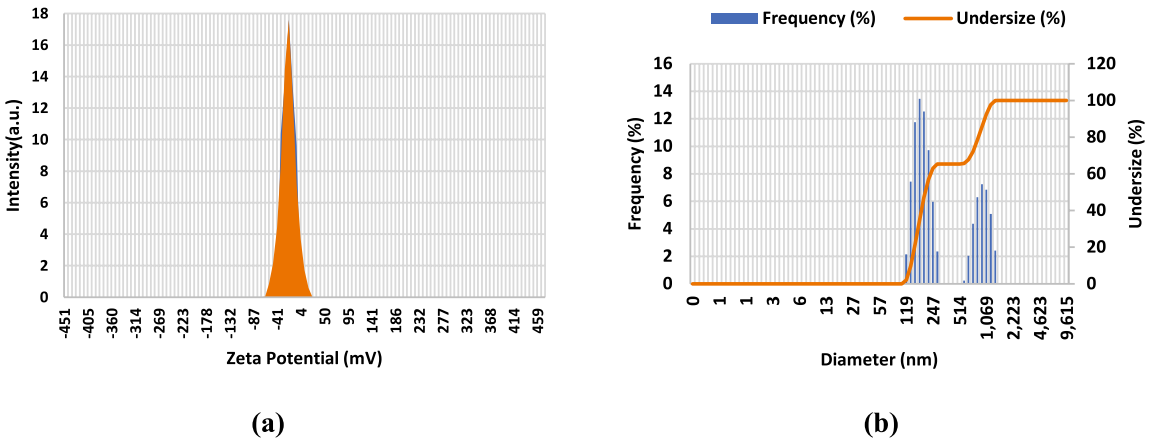

Fig. 3 Zeta analysis of Ag/Cu NC. **a** Zeta potential analysis. **b** DLS analysis

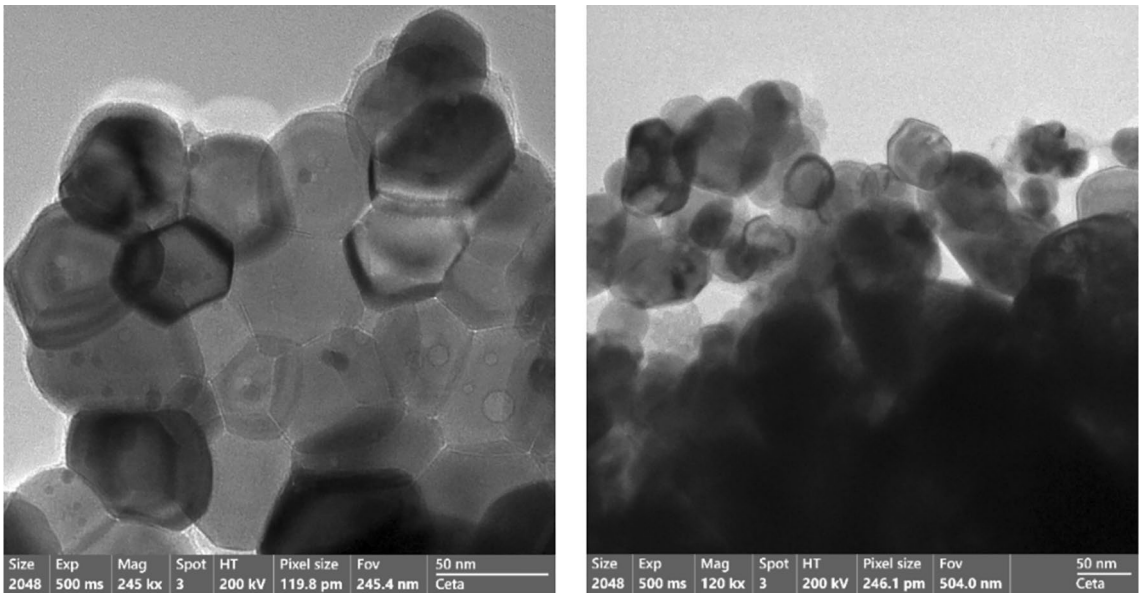

Fig. 4 HR-TEM images of Ag/Cu NC. The images showed well-defined, polyhedral nanoparticles with relatively uniform morphology. The sample was screened at a magnification of 120,000× and 245,000× using a 200 kV accelerating voltage. The scale bar represents 50 nm. The observed contrast and lattice fringes confirm the crystalline nature of the nanostructures, supporting the successful synthesis and integration of silver and copper phases

well-defined crystal structures and highlighting the high crystallinity of the materials.

EDX

Energy-dispersive X-ray analysis of Ag/CuO nanocomposite was carried out to establish the material's elemental composition, which presented carbon, oxygen, copper, and silver signals, as shown in Fig. 5. The analysis revealed clear signals corresponding to carbon (C) (32.7 wt%, 51.12 at%), oxygen (O) (30.26 wt%, 34.37 at%), copper (Cu) (28.46 wt%, 8.08 at%), and silver (Ag) (8.58 wt%, 6.43 at%), confirming the presence of all expected constituents within the nanocomposite. The high carbon content suggests this is due to carbon-based capping agents during synthesis. The notably high carbon content can be attributed to the organic phytochemicals from the *S. latifolium* extract that acted as reducing and stabilizing agents during green synthesis,

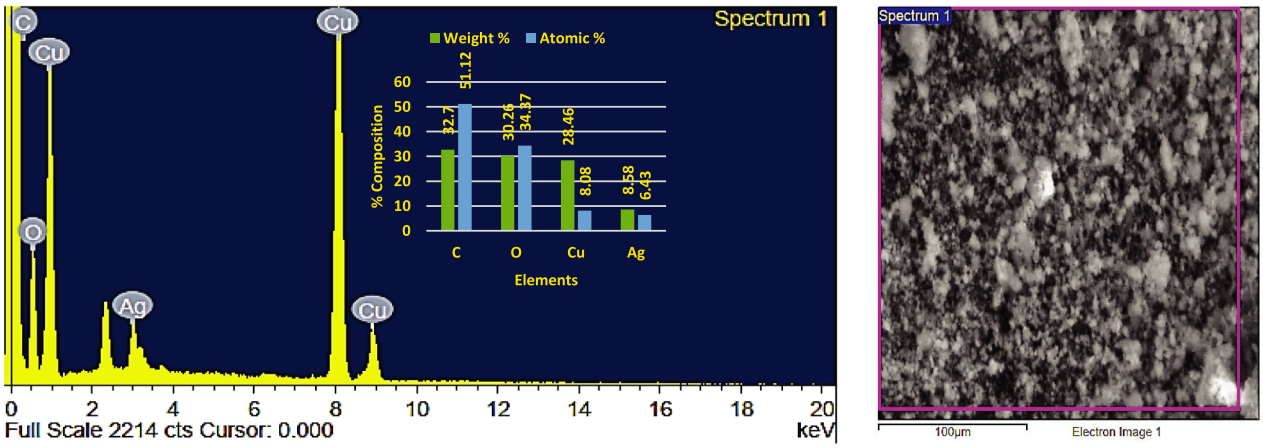

Fig. 5 EDX analysis of Ag/CuO NC

serving as capping agents on the nanoparticle surface. The critical amount of oxygen would hint toward the presence of CuO in the nanocomposite, with copper present in a significant percentage in an oxidized state. Meanwhile, the presence of silver in a detectable but lower concentration confirms its integration as a secondary metallic phase in the bimetallic nanocomposite. In general, EDX results confirm the elemental integrity and suggest a homogeneous distribution of Ag and CuO in the composite.

Scanning electron microscopy (SEM)

The morphological characteristics of the Ag/Cu nanocomposite were investigated using SEM (Fig. 6). The SEM image reveals an agglomerated structure of Ag/Cu nanoparticles, displaying a variety of morphologies comprising a broad range of nanoparticle shapes (spherical, irregular, and slightly elongated). Most particles exhibited an agglomerated structure, forming clusters of different sizes. Individual particles displayed irregular shapes with rough surfaces. Some particles exhibited a more defined, crystalline structure, while others appeared more amorphous. The particle sizes were observed to be in the nanometer range, consistent with the formation of a nanocomposite. The observed agglomeration, with nanoparticles clustering together, indicates how the particles interact, likely due to forces such as van der Waals interactions and surface energy minimization, which is typical in nanoparticle synthesis.

XRD analysis

Figure 7 shows the XRD diffraction pattern of the synthesized Ag/CuO nanocomposite, verifying its crystallinity through numerous distinct peaks. The most intense diffraction

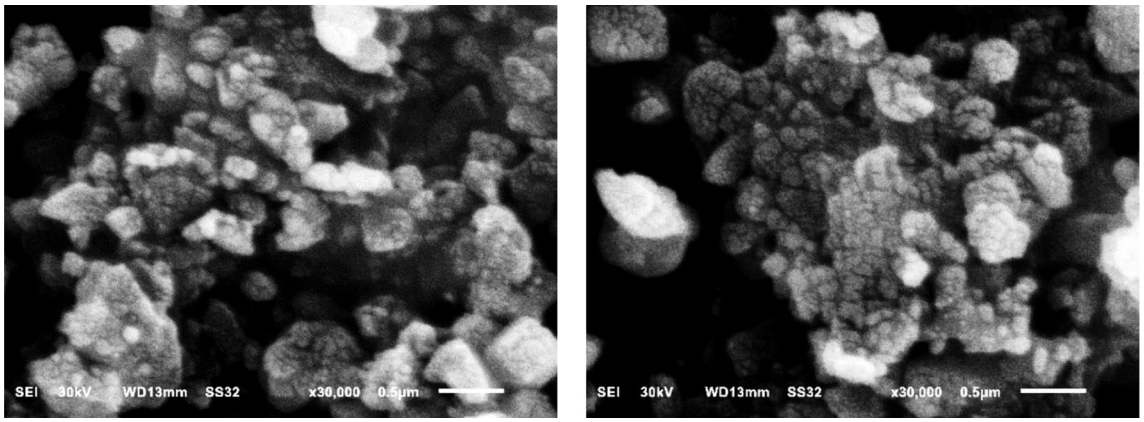

Fig. 6 SEM images of Ag/Cu NC. The images showed well-defined nanoparticles, with spherical, irregular, and slightly elongated nanoparticles. The sample was screened at a magnification of 30,000 × using a 30 kV accelerating voltage. The scale bar represents 0.5 µm

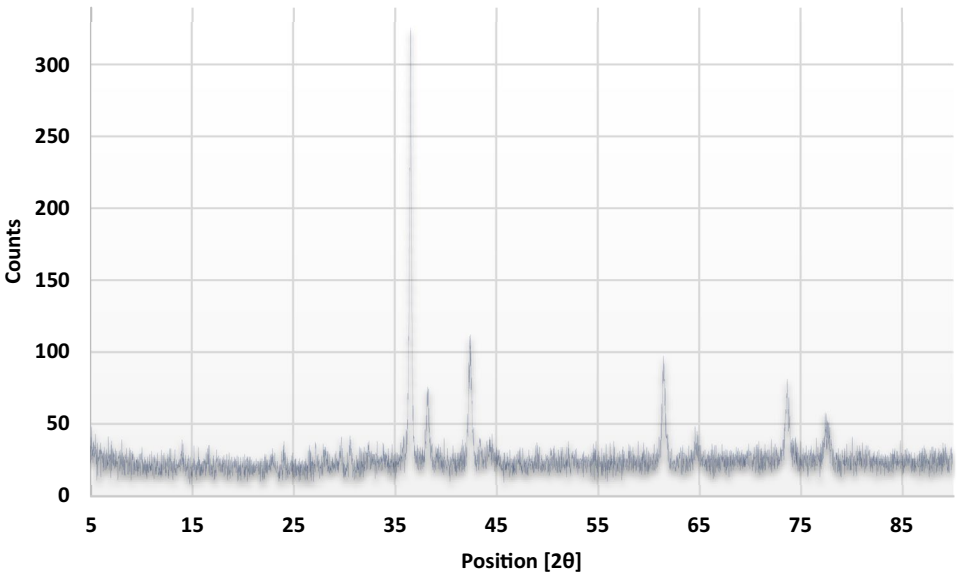

Fig. 7 XRD analysis of Ag/Cu NC

peak appears at 36.565° 2θ, corresponding to a d-spacing of 2.45754 Å with 100% relative intensity and a sharp FWHM of 0.0984°, matched to the CuO reference pattern (JCPDS card no. 03–065-3288), indicating the predominant presence of crystalline copper oxide as the major phase. Additional peaks were recorded at 29.6941° (d = 3.00866 Å, 4.75%), 30.6613° (d = 2.91592 Å, 4.47%), 38.2722° (d = 2.35176 Å, 15.58%), matched to elemental silver (Ag) (JCPDS 01–089-3697), 42.3833° (d = 2.13267 Å, 22.60%), 61.4716° (d = 1.50845 Å, 23.91%), 64.7470° (d = 1.43983 Å, 4.60%), also attributed to Ag, 73.6058° (d = 1.28690 Å, 13.57%), and 77.5487° (d = 1.23001 Å, 7.94%), which matched both CuO and Ag (JCPDS 03–065-3288; 01–089-3697). The presence of these peaks, particularly those associated with Ag at 38.27°, 64.74°, and 77.55°, confirms the formation of silver nanoparticles alongside copper oxide, indicating the successful synthesis of a bimetallic nanocomposite. The relatively narrow FWHM values, especially for the prominent CuO peak, are characteristic of the high crystallinity of the material and its well-ordered lattice. The sharpness and symmetry of the peaks also support uniform crystal growth and phase purity. The XRD results cumulatively confirm the successful green synthesis of Ag/CuO nanocomposites with CuO as the dominant crystalline phase and Ag as an ancillary component incorporated in the structure and functionality of the composite.

To further evaluate the crystalline nature of the synthesized Ag/CuO nanocomposite, the average crystallite size was calculated using Scherrer's equation:

$$D = \frac{K\lambda}{\beta \cos\theta},$$

where D is the crystallite size, K is the shape factor (taken as 0.9), λ is the X-ray wavelength (1.5406 Å for Cu Kα radiation), β is the full width at half maximum (FWHM) of the diffraction peak in radians, and θ is the Bragg angle. Calculations were performed for the major peaks corresponding to the planes at 2θ values of 36.56°, 38.27°, 42.38°, and 61.47°, which showed high relative intensities. The estimated crystallite sizes were approximately 8.9 nm, 4.6 nm, 5.4 nm, and 5.1 nm, respectively, indicating the nanocrystalline nature of the Ag/CuO material. These results confirm that the synthesized nanocomposite consists of well-defined, nanoscale crystalline domains consistent with the observed diffraction patterns.

Phytochemical analysis

The phenolic content in *S. latifolium* extract was found to be 116.79 ± 1.58 mg gallic acid/g dry extract, which was significantly higher than the phenolic content in the Ag/Cu NC (45.91 ± 1.01 mg gallic acid/g dry extract) (Fig. 8). The flavonoid content in *S. latifolium* extract was 46.31 ± 1.35 mg catechin acid/g dry extract, whereas the Ag/Cu NC showed a reduced flavonoid content of 25.32 ± 1.49 mg catechin acid/g dry extract. The tannin content in *S. latifolium* extract was 17.84 ± 2.07 mg tannic acid/g dry extract, while the tannin content in the Ag/Cu NC was 12.25 ± 1.71 mg tannic acid/g dry extract.

Antioxidant activity

Figure 9 depicts the antioxidant results employed using the DPPH free radical scavenging assay for *S. latifolium* extract and Ag/Cu NC. The antioxidant capacity of the samples is directly proportional to the IC_{50} value. *S. latifolium* extract exhibited an IC_{50} value of 0.108 ± 1.54 mg/mL, indicating its significant antioxidant activities. The Ag/Cu NC exhibited

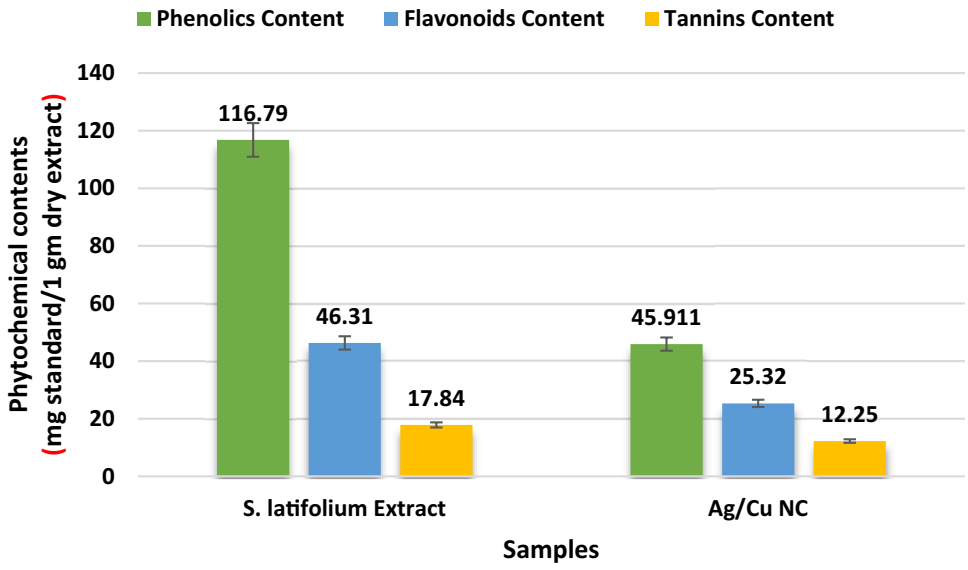

Fig. 8 A comparison of the phytochemical contents of the tested sample

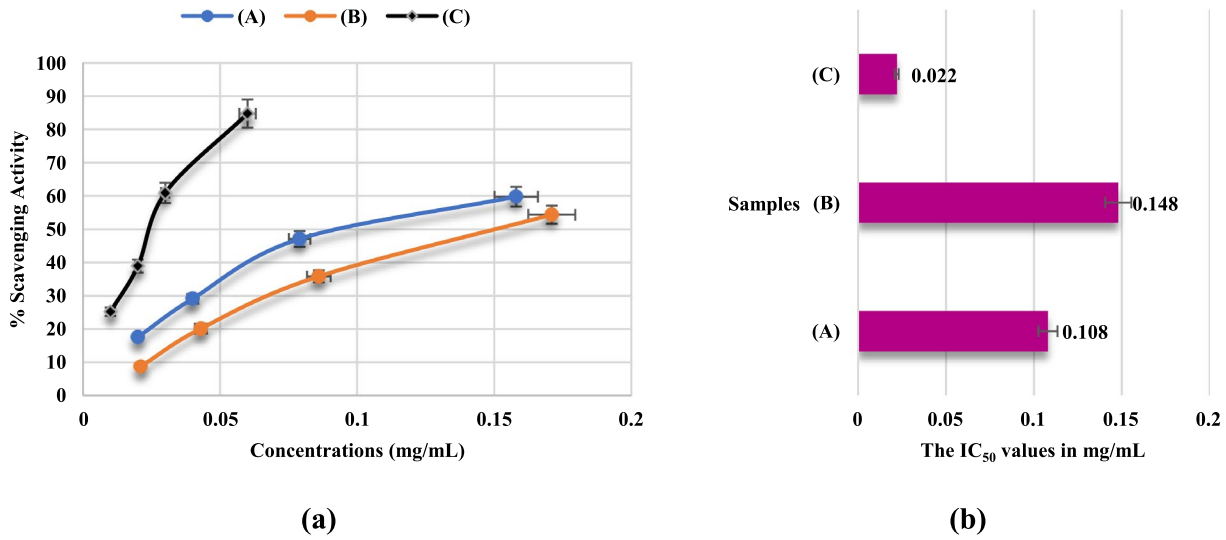

Fig. 9 Antioxidant activity assessed by DPPH assay. **a** IC_{50} values of *S. latifolium* extract (**A**), Ag/Cu nanocomposite (**B**), and ascorbic acid (**C**). **b** % scavenging activity at selected concentrations (0.01–0.1 mg/mL). Error bars represent standard deviation ($n=3$)

the highest IC_{50} at 0.148 ± 1.27 mg/mL, which indicates a general reduction of about 50% in the antioxidant activity of the pure extract. Finally, ascorbic acid was used as the antioxidant standard and expressed the least IC_{50} at 0.022 ± 1.19 mg/mL; thus, it verified its excellence among the samples due to higher free radical scavenging potency. Conversely, a dose-dependent increase in DPPH, with an associated reduction of scavenging activities, was evident in the extract. In the case of extract, its highest scavenging activity, at 0.158 mg/mL, reached up to 59.77 ± 1.01%, which for 0.02 mg/mL reduced to 17.55 ± 1.51%. Similarly, a nanocomposite also showed concentration-dependent tendencies and, at a concentration of 0.171 mg/mL, presented 54.35 ± 1.84%, reducing its scavenging activity at a concentration of 0.021 mg/mL down to 8.70 ± 1.29%. Thus, at each comparative concentration, the scavenging activities were slightly lower than those recorded for the extract.

Antibacterial activity

Agar well diffusion assay

Antibacterial activity for the *S. latifolium* extract and Ag/Cu NC was estimated using the suitable diffusion assay, as shown in Table 1 & Fig. 10. Contrary to our expectation, no inhibitory action of *S. latifolium* extract was observed on any Gram-positive or Gram-negative bacteria.

Table 1 The results of antibacterial activity using a well diffusion assay

Microorganisms	Inhibition zones in mm ± SD			
	S. latifolium extract	Ag/Cu NC	Negative Control (30%, EtOH)	Gentamicin
Gram-negative bacteria				
Escherichia coli	−ve	17.0 ± 1.29	−ve	21.0 ± 0.53
Salmonella typhimurium	−ve	13.0 ± 1.38	−ve	17.0 ± 1.18
Klebsiella pneumonia	−ve	13.0 ± 1.57	−ve	19.0 ± 1.68
Enterobacter cloacae	−ve	15.0 ± 1.07	−ve	11.0 ± 1.94
Gram-positive bacteria				
Bacillus subtilis	−ve	38.0 ± 1.54	−ve	17.0 ± 1.16
Bacillus cereus	−ve	14.0 ± 1.81	−ve	18.0 ± 1.09
Staphylococcus aureus	−ve	14.0 ± 1.29	−ve	17.0 ± 1.44
Staphylococcus epidermidis	−ve	25.0 ± 1.40	−ve	19.0 ± 1.71

The results of inhibition zones in mm are expressed as the mean value ± standard deviation (SD). The experiments were run in triplicate

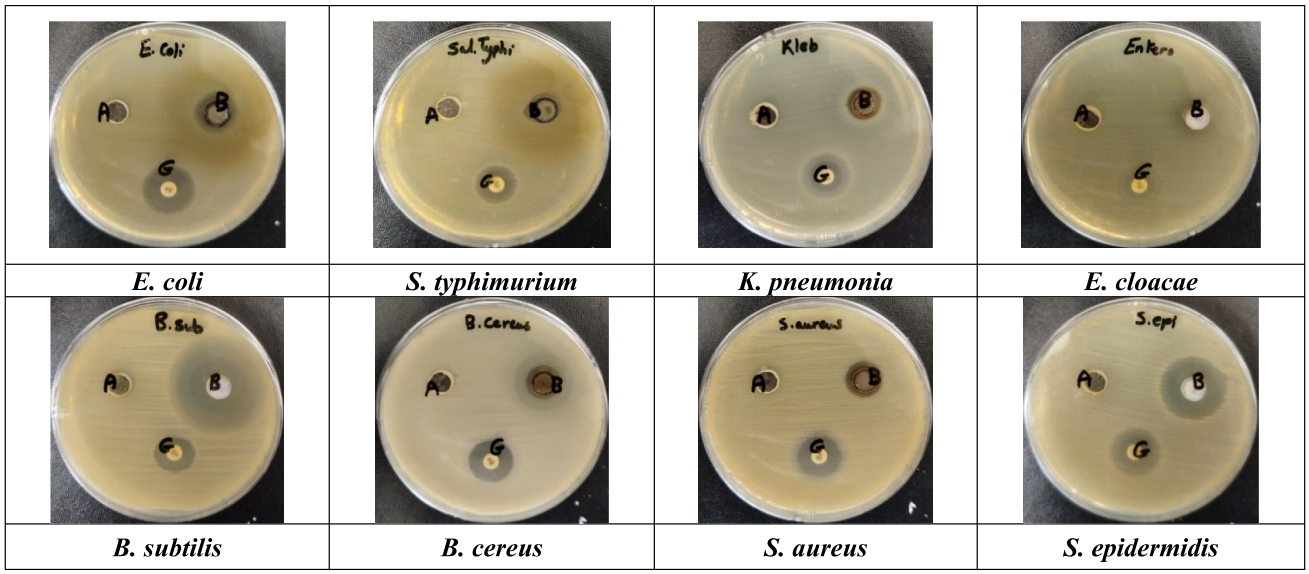

Fig. 10 The Petri dishes images identified the antibacterial activity of the nanocomposites against several pathogenic bacterial species. A refers to algae extract. B refers to Ag/Cu NC, and G refers to Gentamicin

Statistical evaluation of Ag/Cu NC inhibition zone and gentamicin by one-way analysis of variance (ANOVA) and Tukey post-test was carried out to draw the significance of antibacterial activity. It was observed that Ag/Cu NC was highly effective at inhibiting *B. subtilis* ($p < 0.001$) and *S. epidermidis* ($p < 0.01$) than gentamicin. Conversely, no statistical difference was obtained in the zone of inhibition of Gram-negative bacteria, including *E. coli* and *S. typhimurium*, in either gentamicin, which performed equally or even better. The demonstrated results endorse the high and selective antibacterial effects of the synthesized Ag/Cu NC against Gram-positive bacteria.

However, Ag/Cu NC had very prominent antibacterial action against Gram-positive bacteria. The maximum zone of inhibition observed for *B. subtilis* was 38.0 ± 1.54 mm. Other Gram-positive bacteria like *S. Epidermidis* had a mean diameter of the inhibition zone of 25.0 ± 1.40 mm, showing moderate susceptibility. Gram-negative bacteria expressed moderate activities from 13.0 ± 1.38 mm in *S. typhimurium* to 17.0 ± 1.29 mm in *E. coli* for the Ag/Cu NC. Gentamicin constantly showed higher or comparable antibacterial activity in parallel tests, whereas the harmful control-30% ethanol did not express any inhibitive activity.

Minimum inhibitory concentration (MIC)

The Ag/Cu NC MIC was determined against the most potent pathogenic bacteria, as shown in Table 2. The MIC values varied significantly among the tested microorganisms, reflecting differences in their susceptibility. The lowest MIC value was observed for *B. subtilis* (0.692 µg/mL, $OD_{600} = 0.004$), indicating its high sensitivity to the Ag/Cu NC. Similarly, *S. epidermidis* exhibited an MIC of 11.07 µg/mL ($OD_{600} = 0.105$), showing notable susceptibility. For Gram-negative bacteria, *E. coli* had an MIC of 44.3 µg/mL ($OD_{600} = 0.02$), while *E. cloacae* showed the highest MIC value of 177.2 µg/mL ($OD_{600} = 0.012$), indicating reduced sensitivity compared to other tested strains.

Table 2 The MIC results of Ag/Cu NC measured at OD_{600} against the most potent pathogenic bacteria

Microorganism	Concentration (µg/mL)	$O.D_{600}$	Control ($O.D_{600}$)
E. cloacae	177.2	0.012	0.870
E. coli	44.3	0.02	1.113
B. subtilis	0.692	0.004	0.843
S. epidermidis	11.07	0.105	0.975

Mechanism of action against bacterial species

Transmission electron microscopy (TEM) analysis of untreated *Bacillus subtilis* showed that cells of this species had intact cellular structures. Indeed, from the TEM micrograph in Fig. 11a, the bacterial cells featured smooth cell surfaces and well-defined cell boundaries without signs of apparent cellular damage or changes. The cell walls are similarly even, showing no signs of morphological disruption and structural deformation. This will set the baseline for comparing the influence of Ag/Cu nanocomposites on *B. subtilis*.

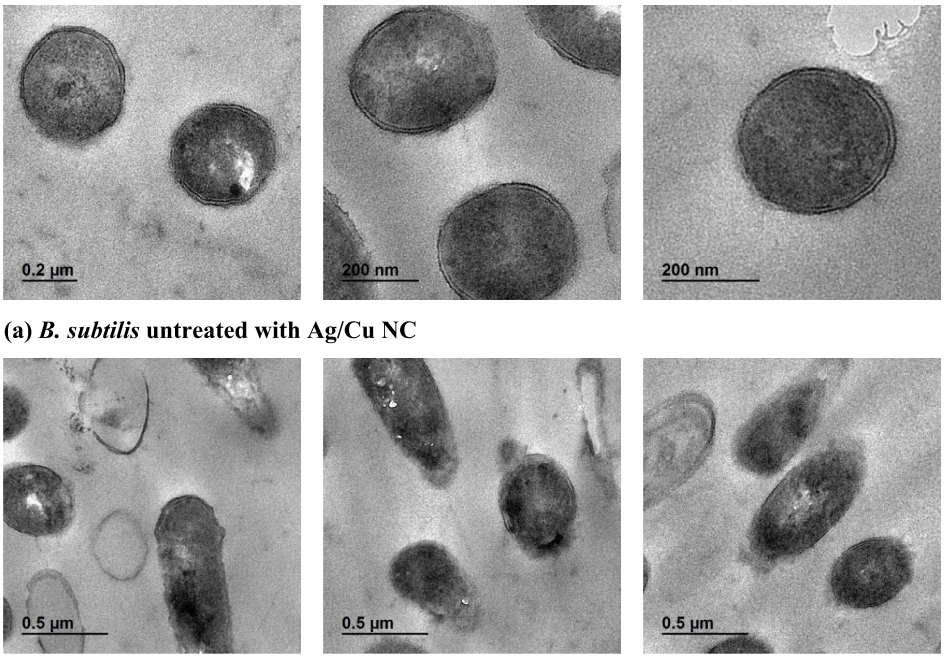

(a) *B. subtilis* untreated with Ag/Cu NC

(b) *B. subtilis* treated with Ag/Cu NC

Fig. 11 TEM micrographs of *Bacillus subtilis* species treated and untreated with Ag/Cu NC

For TEM-analyzability of samples, 0.692 µg/mL concentration of Ag/Cu NC (MIC value) was applied to bacterial cultures for 4 h at 37 ℃ under shaking conditions (150 rpm). The cells were then fixed using 2.5% glutaraldehyde in 0.1 M phosphate buffer (pH 7.4) for 2 h, post-fixed using 1% osmium tetroxide, dehydrated using a graded series of ethanol, and embedded in resin. Thin sections were examined using a TEM (JEOL JEM-2100, Tokyo, Japan) at 200 kV.

The TEM micrographs of the *B. subtilis* species treated with the Ag/Cu nanocomposite show evident morphological changes compared to the untreated cells. The TEM micrograph in Fig. 11b shows that the bacterial cells have disrupted and irregular cell walls, showing visible structural damage. The cytoplasmic content seems to have leaked or degraded in several cells, indicating a compromised cellular membrane. Electron-dense regions, which are believed to be Ag/Cu nanoparticles, were also present on or near the bacterial surface. Furthermore, electron-dense regions, apparently corresponding to Ag/Cu nanoparticles, are positioned close or even attached to the surface of bacteria. These data evidence the active interaction of the nanocomposite with bacterial cells as one of the factors of such nanocomposite structural degradation. The above suggests that the antibacterial activity is likely due to membrane damage, oxidative stress induction, and nanoparticle–cell interaction, leading to the cell death of bacteria.

Anticancer activity assessment

MTT assays revealed a dose-dependent cytotoxicity of the Ag/Cu NC in both HepG2 and HCT116 cell lines, with IC_{50} values of 16.71 µg and 8.17 µg, respectively (Fig. 12). These findings suggest that Ag/Cu NCs exert a significant inhibitory effect on cell viability, with more potent cytotoxicity observed in HCT116 cells compared to HepG2 cells. The results highlight the potential of Ag/Cu NCs in reducing cells through a dose-dependent mechanism. In WI-38 cells, a similar trend was observed, with no significant variation in cytotoxicity across different concentrations, resulting in an IC_{50} value of 84.20 µg. These findings suggest that Ag/Cu NCs do not effectively suppress cell survival in WI-38 cells. However, they demonstrate the potential to inhibit cell viability in cancerous cells, highlighting their promise as effective anticancer agents targeting various cell types.

Exploratory in silico assessment of phytochemical ADME properties

The ADME toxicity results for Ag/Cu NCs demonstrated varying characteristics across the three cell lines (Table 3). Absorption was moderate to high in HepG2 and HCT116 cells, with significant uptake observed at 5–10 µg/mL concentrations. This suggests that cancer cells readily absorbed the nanocomposites. In contrast, WI-38 (normal cells) exhibited low absorption across all concentrations,

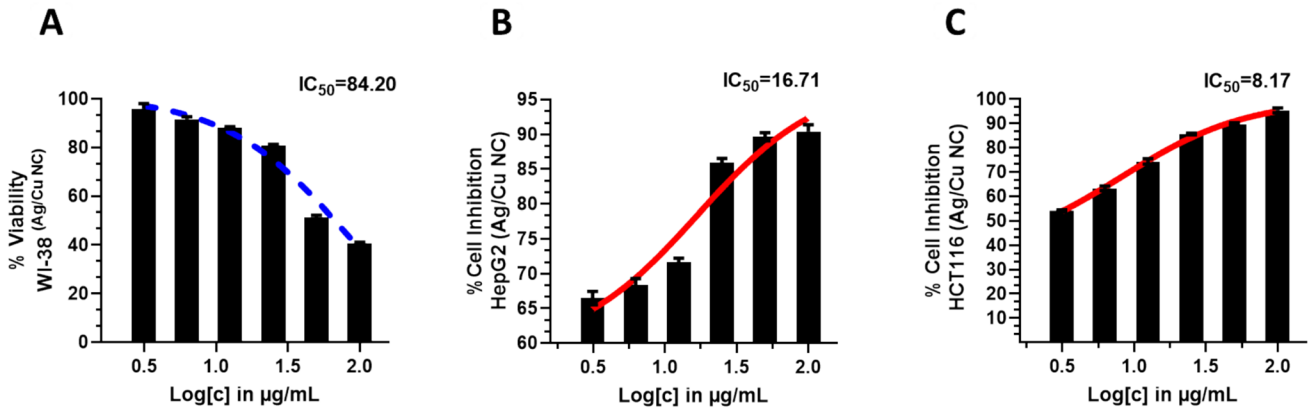

Fig. 12 Cytotoxicity of Ag/Cu NCs in WI-38 Cells, HepG2, and HCT116. Cell viability was assessed by MTT assay after treatment with increasing concentrations of Ag/Cu NCs for 24 h. **A** WI-38 cells exhibited minimal cytotoxicity across all tested concentrations, with an IC_{50} value of 84.20 µg. In contrast, a dose-dependent reduction in cell viability was observed in both **B** HepG2 (liver cancer) and **C** HCT116 (colorectal cancer) cells, with IC_{50} values of 16.71 µg and 8.17 µg, respectively. These results suggest that Ag/Cu NCs effectively suppress cell survival in cancerous cells while showing limited cytotoxicity in normal cells. MTT assays were performed in triplicate ($n=3$) for each concentration and repeated independently three times to ensure reproducibility. IC_{50} was calculated based on non-linear regression sigmoid analysis

Table 3 ADME Toxicities of Ag/Cu NCs in HepG2, HCT116, and WI-38 Cell Lines

Cell Line	Concentration (µg/mL)	Absorption	Distribution	Metabolism	Excretion	IC_{50} (µg/mL)	Cytotoxicity Observed	Toxicological Effects
HepG2 (Liver Cancer)	1	Moderate	High	Moderate	Low	16.71	Low cytotoxicity observed at lower concentrations	Liver cell damage potential: mild metabolic stress
	5	High	High	High	Low		Moderate cytotoxicity observed	Possible interference with liver enzymes
	10	High	Very High	High	Low		Significant cytotoxicity observed	Potential hepatotoxicity; cell apoptosis
HCT116 (Colorectal Cancer)	1	Low	Moderate	Moderate	Low	8.17	Low cytotoxicity observed at lower concentrations	Reduced proliferation; moderate toxicity at higher doses
	5	Moderate	High	High	Low		Moderate cytotoxicity observed	Increased apoptosis; moderate DNA damage
	10	High	High	High	Low		Significant cytotoxicity observed	Potent inhibition of growth; potential genotoxicity
WI-38 (Normal Cells)	1	Low	Low	Low	Low	84.20	Minimal cytotoxicity observed	Minimal toxicity at low concentrations
	5	Low	Low	Low	Low		No significant cytotoxicity	No significant metabolic disturbance
	10	Low	Low	Low	Low		Very low cytotoxicity was observed	Minimal effect on cell survival; low metabolic interference

Absorption: How well the Ag/Cu NCs are absorbed into the cells. Distribution: How the nanocomposites distribute within the cells and tissues. Metabolism: The extent to which the Ag/Cu NCs undergo metabolic transformation in the cells. Excretion: The extent to which the nanocomposites are eliminated from the cells or tissues. IC_{50}: The concentration at which 50% of cell viability is inhibited, indicating cytotoxic potency. Cytotoxicity Observed: The extent of cell viability loss as noted in the IC_{50} values. Toxicological Effects: Observed or potential adverse effects such as apoptosis, DNA damage, or metabolic disturbance

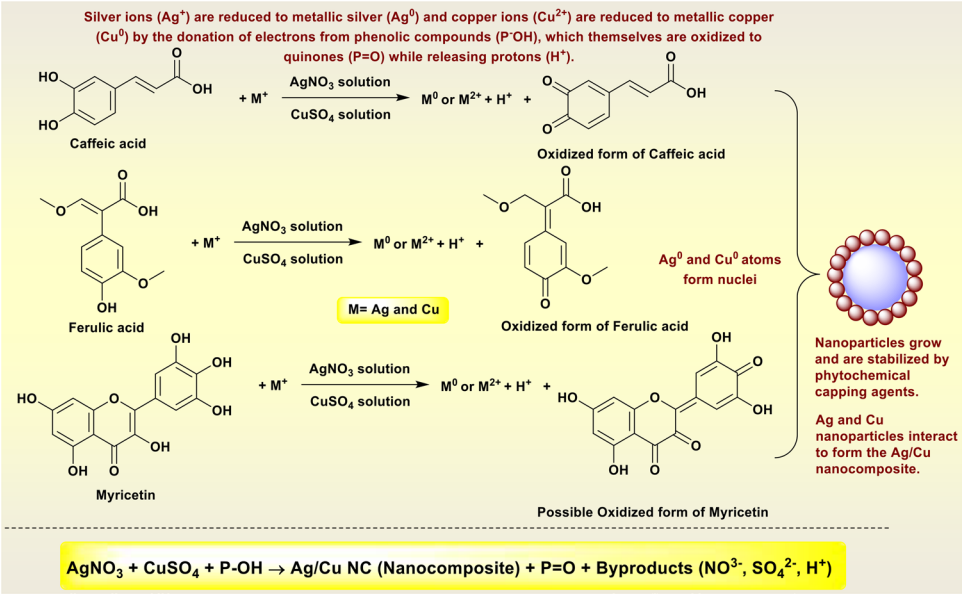

Scheme 1. The plausible mechanism for the formation of Ag/Cu NC

indicating inefficient uptake in normal cells. Regarding distribution, Ag/Cu NCs were highly distributed within HepG2 and HCT116 cells at concentrations of 5 µg/mL and above, suggesting effective permeation across cell membranes. However, WI-38 cells showed low distribution, likely due to the lower uptake and accumulation of Ag/Cu NCs. For metabolism, HepG2 and HCT116 cells showed significant metabolic processing of Ag/Cu NCs, particularly at 10 µg/mL, which suggests that these cells actively metabolize the nanocomposites, potentially leading to interference with cellular metabolic processes. On the other hand, WI-38 cells exhibited minimal metabolism, indicating that normal cells had less interaction with the nanocomposites. These findings provide only preliminary bioactivity profiles of the surface-associated phytochemicals and are not reflective of the entire nanocomposite's behavior. Due to the limitations of current in silico platforms for nanoparticle modeling, these results are intended to inform future hypothesis-driven in vivo validation studies.

Regarding excretion, Ag/Cu NCs exhibited generally low excretion rates across all three cell lines, suggesting that the nanocomposites remain within the cells for extended periods, increasing the potential for prolonged exposure and toxicity, especially in cancer cells. IC_{50} values revealed that Ag/Cu NCs were most toxic to HCT116 cells (8.17 µg/mL), followed by HepG2 cells (16.71 µg/mL), with both cell lines showing dose-dependent cytotoxicity. In contrast, WI-38 cells exhibited minimal cytotoxicity, with an IC_{50} value of 84.20 µg/mL, indicating lower toxicity than normal cells. Toxicological effects observed in HepG2 and HCT116 cells included significant cytotoxicity, apoptosis, cell membrane damage, and potential genotoxicity, evidenced by morphological changes such as cell shrinkage and detachment. Conversely, WI-38 cells exhibited minimal cytotoxicity and no significant metabolic disturbance, suggesting that Ag/Cu NCs pose a lower risk to normal cells.

Discussion

The *S. latifolium* extract has numerous phenolic compounds that are primarily extracted from the natural secondary metabolites of algae. They are caffeic acid, gallic acid, protocatechuic acid, ferulic acid, quercetin, and myricetin, which are responsible for the antioxidant property of the extract [53–55]. Aqueous extract of *S. latifolium* can be justified by a possible mechanism through the participation of polyphenols, flavonoids, and tannins as reducing agents of the silver and copper ions [56]. Phytochemical compounds exhibited a reaction with silver nitrate ($AgNO_3$) and copper sulfate ($CuSO_4$) solutions, in which phytochemicals strip Ag^+ and Cu^{2+} of an electron to deposit them in metallic form (Ag^0 and Cu^0, respectively), while the phytochemicals get one electron each to form quinones [57]. In this route, Ag^+ ions are reduced to Ag^0 and copper ions (Cu^{2+}) to metallic copper (Cu^0) by donating electrons to the phenolic compounds in an effort to create Ag and Cu nanoparticles (Scheme 1). Similarly, these phytochemicals cover the metal nanoparticles on the surface in an effort to protect against coagulation [58]. This process results in the green synthesis of an Ag/Cu NC, in which individual silver and copper nanoparticles are stabilized by capping agents derived from the *S. latifolium* extract. The extract serves a dual function, as both a reducing and stabilizing agent [59], enabling the eco-friendly formation of bimetallic nanomaterials. This mechanism supports

the sustainable fabrication of silver–copper nanocomposites through plant-mediated synthesis.

UV–visible spectra of *S. latifolium* extract and Ag/Cu NC have different bands, revealing characteristic data that supports understanding their nature. The maximum at 506 nm in absorbance value of 0.974 is attributed to the presence of bioactive compounds such as flavonoids and phenolic compounds absorbing in the visible region. This absorption is specific to compounds containing conjugated double bonds or aromatic ring systems that are relatively common in plant extracts. The high absorbance value indicated the high contents of the bioactive molecules in the extract, which contribute to its therapeutic potential, for example, antioxidant and antimicrobial activities [60]. The maximum density occurs at the wavelength 506 nm, which is in the visible spectrum, a feature often ascribed to the chromophoric groups of many plant metabolites. The other absorbance peak located at 782 nm for Ag/Cu NC is attributed to surface plasmon resonance (SPR), the characteristic optical feature of metallic nanoparticles [61]. This is usually experienced in metal nanoparticles such as silver and copper, where free electrons in the metallic surface vibrate in a manner of way when exposed to light. The SPR peak at 782 nm indicates that the Ag/Cu nanoparticles are in the nanoscale range, further confirmed by the high absorbance value of 0.957. This value suggests that the nanocomposites are well formed and have high optical activity [62]. These shifts in the SPR peak position to a longer wavelength (compared to conventional silver nanoparticles, which have SPR bands at around 400–450 nm) could be attributed to the effect of copper in the nanocomposite structure because copper nanoparticles generally have an SPR band at longer wavelengths [63]. Typically, the UV–Vis results indicate the successful synthesis of the Ag/Cu NC and highlight the presence of bioactive compounds in the *S. latifolium* extract. The absorption characteristics observed for *S. latifolium* extract and the Ag/Cu NC are consistent with their expected chemical and structural properties.

The FTIR analysis confirmed the presence of phytochemical components in the *S. latifolium* extract and their involvement in the Ag/Cu NC synthesis. The broad O–H stretching band 3448 cm^{-1} in the extract shifted to 3321 cm^{-1} in the nanocomposite, indicating hydrogen bonding or interaction with the metal nanoparticles [64]. Similarly, the carbonyl stretching bands (C = O) observed at 1662 and 1641 cm^{-1} in the Ag/Cu NC suggest the involvement of polyphenols and flavonoids in reducing and stabilizing the metal ions during the bioreduction process [65]. The appearance of new bands in the Ag/Cu NC, such as those at 545 and 477 cm^{-1}, corresponds to metal–oxygen (M–O) stretching vibrations, confirming the formation of silver and copper nanoparticles [66]. Shifts in bands related to aromatic rings (e.g., 1549 cm^{-1} in the extract and 1464 cm^{-1} in the NC) further support the interaction of phytochemicals with nanoparticles. These findings demonstrate that bioactive compounds in the *S. latifolium* extract reduce metal ions and cap the nanoparticles, stabilizing them. The observed spectral changes emphasize the dual role of phytochemicals in nanoparticle synthesis and highlight the successful integration of plant-derived functional groups into the nanocomposite.

The zeta potential of −19.4 mV for the Ag/Cu NC, which indicates moderate nanoparticle surface charge, was determined. An absolute zeta potential value over + 30 mV or below −30 mV suggests good colloidal stability as these surfaces exhibit high electrostatic repulsion that discourages particle aggregation [67]. In this case, the value of −19.4 mV indicates sufficient electrostatic stability to prevent significant aggregation, although not as strong as more extreme values seen with highly charged particles. This negative charge of the nanocomposite surface might arise from the adsorption of ions or phytochemicals with carboxyl or hydroxyl groups, an electric double layer around the nanoparticles, or electrostatic interactions with other particles or ions [68]. This is supported by the mean electrophoretic mobility of −0.000150 cm^2/Vs, which provides additional evidence as to the transport of the particles when an electric field was applied, further supporting the claim of electrostatic dispersion. The results of the DLS analysis provide insights into the size distribution and dispersion stability of Ag/Cu NC in the colloidal system. The observed size of 430 nm reflects the hydrodynamic diameter of the particles, including any solvation layer and potential aggregation of primary nanoparticles. This size may differ from the actual core size of the Ag/Cu NC as measured by other techniques, e.g., TEM, due to the influence of the surrounding medium and any stabilizing agents. The PDI value of 0.408 indicates that most of the nanoparticles are similar but with minimal variation in the size distribution. Odzak et al. [69] and Zhang et al. [70] stated that for most nanocomposite systems, a PDI value of less than 0.5 is acceptable, more or less suggesting uniform dispersion. Nevertheless, this value also indicates a minimal current heterogeneity, which might be attributed to the nanocomposite synthesis process or agglomerated nanoparticles in the dispersion.

The observed morphological diversity of the Ag/Cu nanoparticles likely arises from the complex interplay of various factors during the synthesis process. The formation of nanoparticles in spherical, hexagonal, and truncated hexagonal shapes can be attributed to differences in nucleation rates and the kinetics of particle growth [71, 72]. Some of them are spherical, while others are hexagonal and truncated hexagonal, indicating that the nanocomposite contains nanoparticles that experience different growth modes. Particle sizes range from a few nanometers to several tens of nanometers. Furthermore, some of the nanoparticles displayed crystalline lattice fringes, pointing

to the synthesized nanomaterials' well-defined crystal arrangement and high crystalline nature. The crystalline lattice fringes in some of the nanoparticles further suggest that most of the Ag/Cu NCs are single crystals or polycrystals with well-defined crystallographic orientations. This aspect of crystallinity is one of the most influential factors for the properties of the nanomaterial, including its optical characteristics and magnetic behavior [73, 74]. Crystalline structures often have superior properties due to their regular atomic structure [75]. This uniformity allows specific interactions, such as the transfer of electrons involved in catalytic reactions or absorptions of radiation in optical applications, to occur reasonably quickly [76, 77].

The EDX analysis of the Ag/CuO NC reveals a composition that suggests a well-balanced integration of carbon, oxygen, copper, and silver. The high carbon content indicates the presence of deposited phytochemical components, commonly used to prevent nanoparticle aggregation and control their size during synthesis [78]. Oxygen, a significant component, confirms the presence of CuO in the nanocomposite, with the atomic percentage of oxygen being higher than copper, suggesting CuO as the dominant phase [79]. The copper content indicates a mixture of metallic copper and copper oxide, while the lower silver content highlights its role as a secondary component, likely contributing to the nanomaterial's enhanced antimicrobial, optical, and electronic properties [80]. Generally, the elemental composition and distribution support the successful formation of a CuO matrix with silver nanoparticles, making the Ag/CuO nanocomposite a promising nanomaterial for various applications, including antimicrobial actions and nanotechnology.

The SEM images revealed the morphological characteristics of the synthesized Ag/Cu nanocomposite. The observed agglomeration of Ag/Cu nanoparticles is a typical phenomenon in nanoparticle synthesis, driven by several factors. Van der Waals forces, weak attractive forces between nanoparticles, can lead to their aggregation, especially when the nanoparticles are close [81]. Additionally, nanoparticles tend to minimize their surface energy by clustering, leading to the formation of agglomerates. The diverse morphologies observed in the SEM images might result from variations in the nucleation and growth stages during synthesis, where the nanoparticles undergo different growth patterns influenced by the synthesis parameters [82]. The presence of both crystalline and amorphous regions suggests that the material may have a mixture of different phases or a degree of structural disorder [83]. The presence of crystalline and amorphous regions could influence its mechanical properties and response to external stimuli [84]. The observed particle size range is consistent with the definition of a nanocomposite, where one or more components have dimensions in the nanometer scale.

The results of XRD analysis confirm that Ag/CuO nanocomposites are crystalline. Peaks correspond to the standard diffraction pattern for both Ag and CuO. Sharp and well-defined peaks, especially at 36.565° 2θ (d-spacing = 2.45754 Å), showed crystalline CuO, which is inferred by its characteristic diffraction pattern [85]. Further evidence of the CuO phase formation peaks at positions such as 29.6941° and 38.2722°, and so on, whereas the presence of Ag is represented through peaks at 64.7470° and 77.5487°, which establish the presence of the two components within the nanocomposite [86, 87]. Besides, from the FWHM values, one may assume a rather good crystallite development; the larger crystal size generally corresponds to narrower peaks, considering its good crystallinity. The presence of several peaks corresponding to various diffraction planes confirms the formation of the composite material, both with Ag and CuO phases. The relative intensity values, particularly the one at 36.565°, confirm the predominance of the CuO phase in the nanocomposite, while the role of silver is secondary. The identification of these phases is further confirmed by several reference matches: 03–065-3288 for CuO and 01–089-3697 for Ag. Abed et al. [88] reported similar findings that aligned with our results, in which monoclinic CuO was the dominant phase in Ag/CuO nanocomposites. In brief, the XRD analysis provides clear evidence for forming a nanocomposite consisting of both Ag and CuO. The sharp, well-defined peaks suggest good crystallinity, with CuO as the primary phase and silver (Ag) as a secondary phase. This confirms the successful synthesis of the Ag/CuO nanocomposite, which may offer enhanced properties due to the synergy between the two components.

The results of the phytochemical analysis revealed a noticeable reduction in the phenolic, flavonoid, and tannin content in the Ag/Cu NC compared to the original *S. latifolium* extract. This reduction can be attributed to the bioreduction process during the Ag/Cu NC synthesis. The significant decrease of the phytochemical content, particularly the phenolics, the flavonoids, and the tannins in Ag/Cu nanocomposite in relation to *Sargassum latifolium* extract (Fig. 8), can be explained by their active participation in the biosynthesis process. These phytochemicals acted as reducing and stabilizing agents in the green synthesis of the nanocomposite. Most notably, phenolic and flavonoid compounds reduce Ag^{+} and Cu^{2+} to nano-level particles and cap and stabilize the resultant nanostructures. Consequently, many such phytochemicals are either converted into chemical or structural structures in the nanoparticle surfaces or are converted into NC with reduced free concentrations. This decrease establishes that they were indeed active participants in the formation of nitrogen-based nanoparticles and lends further credence to the green synthesis method, which was successfully used in this experiment. This explanation aligns with recent literature [39, 41, 44, 45], which reports

that bioactive compounds such as phenolics and flavonoids play a crucial role in nanoparticle synthesis by donating electrons to reduce metal ions into their nanoparticle form. Such participation in the bioreduction process diminishes their concentration in the resultant nanomaterial solution. Despite the reduction, the residual levels of phenolic, flavonoid, and tannin contents in the Ag/Cu NC suggest that these compounds are partially retained and might contribute to their bioactivity [89, 90]. Additionally, the presence of metal nanoparticles in the composite may synergize with the retained phytochemicals, potentially enhancing its overall biological properties.

The antioxidant results revealed a very explicit concentration-dependent behavior in all tested samples. In each case, *S. latifolium* extract has given higher scavenging activity at its equivalent concentration than the Ag/Cu NCs. Therefore, the observed trend in scavenging activity for the nanocomposite supports the lower content of phytochemicals recorded in the current study after nanoparticle synthesis. This is supported by recent literature [91, 92], in which the mechanism involves using antioxidant compounds as reducing agents in forming and stabilizing silver and copper nanoparticles, hence reducing their availability in the final nanocomposite. The modest decline in free radical scavenging ability in the nanocomposite can be attributed to the lower concentration of free antioxidant phytochemicals.

Despite this reduction, the antioxidant activity of Ag/Cu NC remains notable; it is probably brought about by the synergistic effect of residual phytochemicals and intrinsic properties of silver and copper nanoparticles, both showing antioxidant potential. However, the antioxidant capacities of *S. latifolium* extract and its Ag/Cu NC are comparable. Although *S. latifolium* extract and Ag/Cu NC were not as robust as ascorbic acid, they have shown great promise, considering the additional benefits of their bioactive components and nanostructures, respectively. Results emphasize using *S. latifolium* extract as a natural source of antioxidants, while Ag/Cu NC proved to be one of the hybrid antioxidant systems. The interaction between the phytochemical components of the *S. latifolium* extract and the Ag/Cu NC with DPPH radicals further elucidates their antioxidant mechanisms. These phytochemicals are well known for their ability to donate electrons or hydrogen atoms, effectively neutralizing DPPH radicals [93]. This accounts for the vigorous antioxidant activity of the extract. Within the Ag/Cu NC, phytochemical compounds serve as reducing agents during nanoparticle synthesis and as stabilizers, forming a protective layer around the nanoparticles, which reduces their free concentration and scavenging activity compared to the extract [94]. However, the retained phytochemicals and the inherent antioxidant properties of Ag/Cu NC create a synergistic effect in the Ag/Cu NC. The high surface reactivity of the nanoparticles enhances electron transfer, complementing the activity of the phytochemicals [95]. This interaction underscores the potential of the Ag/Cu NC as an innovative antioxidant system, combining the bioactivity of plant-derived compounds with the unique properties of nanomaterials, making it a valuable candidate for biomedical and environmental applications.

The antibacterial results highlight the potent properties of the Ag/Cu NC, particularly against Gram-positive bacteria. The absence of activity in the *S. latifolium* extract suggests that its bioactive compounds, while necessary in other perspectives like antioxidant activity, do not exhibit significant antibacterial properties in their free form. However, during the bioreduction process, these compounds likely participate in nanoparticle synthesis, contributing to the enhanced antibacterial activity of the Ag/Cu NC [96]. The higher efficiency of the Ag/Cu NC against Gram-positive bacteria may be linked to the bacterial cell wall structure [97]. Gram-positive bacteria, having a thick peptidoglycan layer, probably interact more effectively with nanoparticles, leading to structural damage and disruption of cell metabolism [98]. The relatively lower activity against Gram-negative bacteria, which have more complicated outer membranes, would suggest that even though nanoparticles can penetrate the cell membrane, they are less effective in causing significant cell damage than Gram-positive bacteria [99]. The antibacterial action of Ag/Cu NCs is most probably realized through several mechanisms, such as direct interaction with bacterial membranes [100], the generation of ROS via the release of silver and copper ions [101], and synergistic effects between the two metals [102]. Although gentamicin generally exhibited higher activity, the Ag/Cu NC demonstrated competitive efficacy against some Gram-positive strains and may position it as a complementary or alternative agent to traditional antimicrobials. These findings highlight the importance of using phytochemical-mediated nanoparticle synthesis to develop new antimicrobial systems that will combine natural compound bioactivity with unique features of nanomaterials.

MIC results clearly showed high antibacterial activity of Ag/Cu NC, strongly dependent on the bacterial species. The highest sensitivity was observed for Gram-positive bacteria, especially *B. subtilis*, probably because a thick peptidoglycan layer dominates their more straightforward cell wall composition [103]. This may promote the interaction with Ag/Cu NC and membrane disruption, leading to the death of the bacteria [104]. Furthermore, another Gram-positive bacterium, *S. epidermidis*, showed remarkable sensitivity and thus confirmed the efficacy of Ag/Cu NC against the bacterial group. On the other hand, the Gram-negative bacteria, such as *E. coli* and *E. cloacae*, gave higher MIC values, showing lower susceptibility. This explanation for variation may relate to the complex structure of the outer membrane in Gram-negative bacteria, which act as a barrier for nanoparticles to enter and hence show their further antibacterial

effect [99]. However, the obtained MIC values still indicate growth inhibition by the nanocomposite, establishing it as a potential effective antimicrobial agent.

Such activity is likely a result of combined mechanisms, including the release of reactive oxygen species, interaction with bacterial membranes, which causes structural damage, and interference with cellular processes by silver and copper ions [105, 106]. The low values of MIC obtained for some strains, especially for *B. subtilis*, confirm the potential of Ag/Cu NC for bacterial infection control applications. Results support exploring nanoparticle-based systems as promising alternatives or complementary to conventional antibiotics, especially in the case of resistant pathogens.

TEM studies of *B. subtilis* strains untreated with Ag/Cu NC revealed bacterial cells' structural integrity and morphological normalcy. The smooth and intact outline of cell walls indicates that under untreated conditions, the physiological state of bacterial cells remains without external stress or influence. That would be an essential premise for understanding the further effects of treatments with Ag/Cu NC. The untreated cells are employed as controls in the actual assessment of the level of structural and morphological alterations by the nanocomposites in interaction with bacteria. Various studies reported in the literature assert that the interaction of bacterial species with such metallic nanocomposite materials, for example, Ag or Cu-based materials, led to bacterial disorganization, membrane leakage, and cell lysis ordinarily took place [107, 108]. However, the lack of such features in untreated cells confirms the absence of external nanomaterial interference, highlighting the importance of baseline comparisons in such studies.

From the above information, mechanical and biochemical destruction of bacterial cells could be attributed to the action of the Ag/Cu nanocomposite, causing leakage of the cytoplasmic content and deformation of the cell wall [109]. The electron-dense regions near the bacteria's surface show that nanoparticles interact directly with the bacterial cell membrane, which could promote membrane permeability or oxidative stress [110]. In high probability, the mechanism of bacterial cell damage by Ag/Cu NC is multi-mechanistic. The released Ag and Cu ions can interact with protein thiol groups, disrupt cellular enzymes, and generate reactive oxygen species (ROS) that will eventually cause oxidative stress and cell death [111–113]. The TEM micrographs bring out mechanisms that conform to these expectations. Moreover, it is possible to suggest that penetration of nanoparticles inside the bacterial cell or binding to the membrane potentially leads to additional disruption and intracellular damage [114]. Indeed, the comparison with untreated cells confirms the role of the Ag/Cu NC in the degradation of bacteria. Untreated cells showed a smooth and intact membrane, but in treated cells, precise evidence of morphological and structural damage was shown. This demonstrates the potential for Ag/Cu NC to be compelling enough to suppress *B. subtilis* and possibly other bacterial species.

The MTT assay results demonstrated that Ag/Cu NCs exhibited a dose-dependent cytotoxic effect, with significant inhibition of viability observed in both HepG2 ($IC_{50} = 16.71$ µg/mL) and HCT116 ($IC_{50} = 8.17$ µg/mL) cancer cell lines. In contrast, the viability of normal WI-38 fibroblasts was much less affected ($IC_{50} = 84.20$ µg/mL), suggesting preferential cytotoxicity toward malignant cells. According to NIH/National Cancer Institute (NCI) guidelines, compounds with IC_{50} values below 20 µg/mL are considered to exhibit strong cytotoxic potential against cancer cells, and those with IC_{50} values < 10 µg/mL are typically classified as promising anticancer candidates in preliminary in vitro screening assays [115]. Based on these benchmarks, the Ag/Cu NCs investigated in this study demonstrate potent anticancer activity, particularly against the colorectal HCT116 line.

This selective toxicity profile aligns with several previous studies on nanoparticles, where nanocomposites exhibited enhanced cytotoxic effects in cancer cell lines compared to normal cells. For instance, in studies using silver-based nanoparticles, HepG2 and HCT116 cells were consistently more susceptible to treatment than normal cell lines like WI-38 or other fibroblasts, with IC_{50} values in the range of 10–50 µg/mL in cancer cells and much higher IC50 values in normal cells [115].

In one study by Fierascu et al. [116], AgNPs exhibited similar selective cytotoxicity in HepG2 and HCT116 cells, where cancer cells showed significant decreases in viability at concentrations as low as 10 µg/mL, with normal cell lines (like WI-38) displaying higher resistance to the nanomaterials. Our study corroborates these findings, confirming the selective anticancer activity of Ag/Cu NCs. This selective toxicity may be attributed to cancer cells' differential uptake and metabolism, which are often more permeable to nanoparticles than normal cells [117, 118].

The absorption results from this study show that HepG2 and HCT116 cells absorbed Ag/Cu NCs at higher rates than WI-38 cells, with significant uptake observed at concentrations between 5 and 10 µg/mL. This is consistent with earlier studies on silver and copper-based nanoparticles, where cancerous cells demonstrated higher nanoparticle uptake due to differences in cell membrane permeability compared to normal cells [119]. El-Zayat et al. [120] revealed that HepG2 cells had increased uptake of silver nanoparticles due to their enhanced membrane permeability, while normal fibroblasts (like WI-38) had lower absorption rates.

The distribution of Ag/Cu NCs was high in HepG2 and HCT116 cells, especially at concentrations of 5 µg/mL and above. This mirrors the results seen in other studies involving metal-based nanoparticles. For instance, Xue et al. [121] found that silver nanoparticles were widely distributed within cancer cell lines such as HepG2, leading to

intracellular accumulation and enhanced cytotoxic effects. In contrast, the low distribution observed in WI-38 cells aligns with previous findings that suggest normal cells are less prone to the accumulation of metal nanoparticles, potentially due to slower or lower endocytic activity [122].

The metabolic processing of Ag/Cu NCs was higher in HepG2 and HCT116 cells, particularly at 10 µg/mL, indicating active metabolism of nanocomposites by these cancer cells. This aligns with previous studies showing enhanced nanoparticle metabolism in cancer cells. For example, Raja et al. [123] observed that HepG2 and HCT116 cells exhibited more active metabolic pathways, facilitating nanoparticle transformation and associated toxicity. In contrast, WI-38 cells showed lower metabolism, consistent with reports that normal cells exhibit limited metabolic interaction with nanoparticles [123]. The excretion of Ag/Cu NCs was low across all cell lines, suggesting prolonged intracellular retention post-internalization. This agrees with studies reporting slow excretion of metal nanoparticles, leading to extended exposure and potential toxicity in cancer cells [124]. WI-38 cells exhibited minimal excretion, likely due to reduced internalization and interaction with excretory pathways, resulting in lower toxicity exposure. Toxicological effects, including apoptosis, cell membrane damage, and morphological changes like shrinkage and detachment, were observed in HepG2 and HCT116 cells at higher Ag/Cu NC concentrations, as indicated by MTT assay results. These findings are consistent with earlier studies, such as Hamida et al. [125], which reported apoptosis and membrane blebbing in HepG2 cells exposed to silver nanoparticles [125]. Conversely, WI-38 cells exhibited minimal cytotoxicity and no significant metabolic disturbance, corroborating previous findings on the lower susceptibility of normal cells to nanoparticle toxicity [126].

Limitations

Although this study shows effective green synthesis and multifunctionality bioactivity of Ag/Cu bimetallic nanocomposites derived from *S. latifolium*, there are some limitations to be identified. To begin with, this study lacks a direct comparative study with monometallic Ag NPs and Cu NPs that would be very important to confirm the synergistic effects of the bimetallic system. Second, antibacterial testing excludes time-kill kinetics, synergy tests, or MBC determinations, limiting interpretation of bactericidal potency. Moreover, although TEM was used for nanoparticle characterization, no cellular uptake studies or imaging of nanoparticles in mammalian cells were conducted, which would be central to understanding intracellular mechanisms. The cytotoxicity evaluation relied solely on the MTT assay, which measures metabolic activity but does not distinguish between different modes of cell death (apoptosis, necrosis, or autophagy). As such, any interpretation regarding apoptosis or anticancer mechanisms remains speculative, and further investigation using Annexin V/PI staining, caspase activation assays, nuclear morphology imaging, or gene expression analysis is needed to confirm the pathways involved. Further, while reduced viability was observed in cancer cells (HepG2 and HCT116) compared to normal WI-38 cells, this study lacks comprehensive selectivity profiling across a broader panel of normal and malignant cell lines. Lastly, although our study included an in silico ADME assessment, we recognize the limitations of applying SwissADME and admetSAR—tools designed for small organic molecules—to nanomaterials such as Ag/Cu NCs. Accordingly, these tools were only used to model representative bioactive phytochemicals associated with the nanoparticle surface rather than the entire nanocomposite structure. However, these computational outputs cannot capture key nanoparticle-specific behaviors, such as protein corona formation, endocytic uptake, or long-term biodistribution. Future work will require in vivo pharmacokinetic studies and cellular uptake assays to establish the full ADME and toxicity profile of Ag/Cu NCs in biological systems. This clarification ensures a more accurate interpretation of the data and avoids overextension of conclusions based solely on small-molecule prediction tools.

Conclusion

This study explores the synthesis, characterization, and bioactivity of Ag/Cu NC greenly synthesized using *S. latifolium* extract. The FTIR analysis revealed the involvement of phytochemicals in metal ion reduction and stabilization, evidenced by shifts in functional group bands and metal–oxygen vibrations at 545 and 477 cm^{-1}. Zeta potential revealed a moderate colloidal stability (−19.4 mV), DLS revealed an average particle size of 248.7 nm (PDI = 0.408), while EDX and XRD confirmed a CuO-dominant phase (28.46 wt%) with crystalline structures featuring both copper oxide and silver components. The phytochemical analysis highlighted significant reductions in phenolic (116.79 ± 1.58 to 45.91 ± 1.01 mg gallic acid/g DS), flavonoid (46.31 ± 1.35 to 25.32 ± 1.49 mg catechin/g/g DS), and tannin (17.84 ± 2.07 to 12.25 ± 1.71 mg tannic acid/g DS) contents. Despite this reduction, Ag/Cu NC retained antioxidant potential, with an IC_{50} value of 0.148 ± 1.27 mg/mL compared to the extract's 0.108 ± 1.54 mg/mL. Antibacterial activity was significantly enhanced in Ag/Cu NC, showing inhibition zones of 38.0 ± 1.54 mm for *B. subtilis* and 25.0 ± 1.40 mm for *S. epidermidis*, and a MIC of 0.692 µg/mL for *B. subtilis*. These findings demonstrate the potential of Ag/Cu NC as a novel hybrid antioxidant–antibacterial system, integrating the bioactivity of natural phytochemicals with the functional

properties of nanomaterials, paving the way for applications in medicine and environmental fields. Further, the findings of this study corroborate the selective toxicity of Ag/Cu NCs toward cancer cells, particularly HepG2 and HCT116 cells, while showing minimal toxicity to WI-38 normal cells. The ADME toxicity results provide insight into the mechanisms of action, suggesting that enhanced absorption, distribution, and metabolism in cancer cells contribute to the higher cytotoxicity of Ag/Cu NCs. These results align with previous studies on metal nanoparticles and support the potential of Ag/Cu NCs as promising anticancer agents with low risk to normal cells. Further studies are needed to fully elucidate the molecular mechanisms behind this selective toxicity and optimize the use of Ag/Cu NCs in cancer therapy.

Acknowledgements Princess Nourah bint Abdulrahman University Researchers Supporting Project number (PNURSP2025R446), Princess Nourah bint Abdulrahman University, Riyadh, Saudi Arabia.

Author contributions Conceptualization, Alaa Elmetwalli, Ashraf Elsayed, Khaled M. Elattar, Othman R Alzahrani; Formal analysis, Abeer A. Ghoniem, Mervat G. Hassan, Sara Abdelsayed, Ahmed A. Zaher, Deema Kamal Sabir, Ashraf Elsayed; Investigation, Khaled M. Elattar, Alaa Elmetwalli, Othman R. Alzahrani, Abeer A. Ghoniem, Mervat G. Hassan, Sara Abdelsayed, Ahmed A. Zaher, Deema Kamal Sabir, Ashraf Elsayed; Project administration, Alaa Elmetwalli, Ashraf Elsayed, Khaled M. Elattar, Othman R Alzahrani; Software, Sara Abdelsayed, Ahmed A. Zaher, Deema Kamal Sabir, Ashraf Elsayed; Validation Khaled M. Elattar, Alaa Elmetwalli, Othman R. Alzahrani, Abeer A. Ghoniem, Mervat G. Hassan; Visualization, Alaa Elmetwalli, Ashraf Elsayed, Khaled M. Elattar; Writing—original draft, Alaa Elmetwalli, Khaled M. Elattar; Writing—review and editing, Alaa Elmetwalli.; All authors have read and agreed to the published version of the manuscript.

Funding No funding.

Data availability Data is provided within the manuscript or supplementary information files.

Declarations

Competing interests The authors declare no competing interests.

Ethical approval and consent to participate Not applicable.

Consent for publication Not applicable.

References

1. Luque-Jacobo CM, Cespedes-Loayza AL, Echegaray-Ugarte TS, Cruz-Loayza JL, Cruz I, de Carvalho JC, Goyzueta-Mamani LD. Biogenic synthesis of copper nanoparticles: a systematic review of their features and main applications. Molecules. 2023;28(12):4838.
2. Tiwari M, Jain P, Hariharapura RC, Narayanan K, Bhat U, Udupa N, Rao JV. Biosynthesis of copper nanoparticles using copper-resistant Bacillus cereus, a soil isolate. Process Biochem. 2016;51(10):1348–56.
3. Abdelbasir SM, McCourt KM, Lee CM, Vanegas DC. Waste-derived nanoparticles: synthesis approaches, environmental applications, and sustainability considerations. Front Chem. 2020;8:782.
4. Singh J, Dutta T, Kim KH, Rawat M, Samddar P, Kumar P. 'Green 'synthesis of metals and their oxide nanoparticles: applications for environmental remediation. J Nanobiotechnol. 2018;16:1–24.
5. Rana A, Yadav K, Jagadevan S. A comprehensive review on green synthesis of nature-inspired metal nanoparticles: mechanism, application and toxicity. J Clean Prod. 2020;272:122880.
6. El-Rafie HM, El-Rafie M, Zahran MK. Green synthesis of silver nanoparticles using polysaccharides extracted from marine macro algae. Carbohyd Polym. 2013;96(2):403–10.
7. Hano C, Abbasi BH. Plant-based green synthesis of nanoparticles: Production, characterization, and applications. Biomolecules. 2021;12(1):31.
8. Jadoun S, Arif R, Jangid NK, Meena RK. Green synthesis of nanoparticles using plant extracts: a review. Environ Chem Lett. 2021;19(1):355–74.
9. Bai B, Saranya S, Dheepaasri V, Muniasamy S, Alharbi NS, Selvaraj B, Undal VS, Gnanamangai BM. Biosynthesized copper oxide nanoparticles (CuO NPs) enhances the anti-biofilm efficacy against *K. pneumoniae* and *S. aureus*. J King Saud Univ Sci. 2022;34(6):102120.
10. Devipriya D, Roopan SM. *Cissus quadrangularis* mediated ecofriendly synthesis of copper oxide nanoparticles and its antifungal studies against *Aspergillus niger*, *Aspergillus flavus*. Mater Sci Eng, C. 2017;80:38–44.
11. Mejía-Méndez JL, Sánchez-Ante G, Cerro-López M, Minutti-Calva Y, Navarro-López DE, Lozada-Ramírez JD, Bach H, López-Mena ER, Sánchez-Arreola E. Green synthesis of silver nanoparticles with extracts from Kalanchoe fedtschenkoi: characterization and bioactivities. Biomolecules. 2024;14(7):782. https://doi.org/10.3390/biom14070782.
12. Rajeshkumar S, Menon S, Kumar SV, Tambuwala MM, Bakshi HA, Mehta M, Satija S, Gupta G, Chellappan DK, Thangavelu L, Dua K. Antibacterial and antioxidant potential of biosynthesized copper nanoparticles mediated through *Cissus arnotiana* plant extract. J Photochem Photobiol, B. 2019;197:111531.
13. Vincent J, Lau KS, Evyan YCY, Chin SX, Sillanpää M, Chia CH. Biogenic synthesis of copper-based nanomaterials using plant extracts and their applications: current and future directions. Nanomaterials. 2022;12(19):3312.
14. Arfat YA, Ahmed J, Jacob H. Preparation and characterization of agar-based nanocomposite films reinforced with bimetallic (Ag-Cu) alloy nanoparticles. Carbohyd Polym. 2017;155:382–90.
15. Arfat YA, Ejaz M, Jacob H, Ahmed J. Deciphering the potential of guar gum/Ag-Cu nanocomposite films as an active food packaging material. Carbohyd Polym. 2017;157:65–71.
16. Alavi M, Karimi N. Antiplanktonic, antibiofilm, antiswarming motility and antiquorum sensing activities of green synthesized Ag-TiO2, TiO2-Ag, Ag-Cu and Cu-Ag nanocomposites against multi-drug-resistant bacteria. Artif Cells Nanomed Biotechnol. 2018;46(sup3):399–413.
17. Enrique RA, Nordlund K, Averback RS, Bellon P. Simulations of dynamical stabilization of Ag-Cu nanocomposites by ion-beam processing. J Appl Phys. 2003;93(5):2917–23.
18. Jang J, Lee JM, Oh SB, Choi Y, Jung HS, Choi J. Development of antibiofilm nanocomposites: Ag/Cu bimetallic nanoparticles synthesized on the surface of graphene oxide nanosheets. ACS Appl Mater Interfaces. 2020;12(32):35826–34.
19. Hsieh JH, Yeh TH, Li C, Chiu CH, Huang CT. Antibacterial properties of TaN-(Ag, Cu) nanocomposite thin films. Vacuum. 2013;87:160–3.

20. Doolotkeldieva T, Bobusheva S, Zhasnakunov Z, Satybaldiev A. Biological activity of Ag and Cu monometallic nanoparticles and Ag-Cu bimetallic nanocomposites against plant pathogens and seeds. J Nanomater. 2022;2022(1):1190280.
21. Shahmoradi S, Shariati A, Amini SM, Zargar N, Yadegari Z, Darban-Sarokhalil D. The application of selenium nanoparticles for enhancing the efficacy of photodynamic inactivation of planktonic communities and the biofilm of *Streptococcus mutans*. BMC Res Notes. 2022;15(1):84. https://doi.org/10.1186/s13104-022-05973-w.
22. Sharifkazemi H, Amini SM, Koohi Ortakand R, Narouie B. A review of photodynamic therapy in different types of tumors. Transl Res Urol. 2022;4(2):61–70. https://doi.org/10.22034/tru.2022.337411.1108.
23. Neshastehriz A, Hormozi-Moghaddam Z, Kichi ZA, Taheri SM, Amini SM, Aghaei A. Overcoming breast cancer cell treatment resistance by optimizing sonodynamic therapy and radiation sensitizers on lncRNA PVT1 and miR-1204 expression. Photodiagn Photodyn Ther. 2025;51:104433. https://doi.org/10.1016/j.pdpdt.2024.104433.
24. Amini SM, Rezayat SM, Dinarvand R, Kharrazi S, Jaafari MR. Gold cluster encapsulated liposomes: theranostic agent with stimulus triggered release capability. Med Oncol. 2023;40(5):126. https://doi.org/10.1007/s12032-023-01991-1.
25. Oroskhani N, Amini SM, Shirvalilou S, Khodaie M, Mahdavi SR. Anti-Proliferative activity of Poloxamer cobalt ferrite nanoparticles against human prostate cancer (DU-145) cells: in-vitro study. IET Nanobiotechnol. 2024;2024(1):8929168. https://doi.org/10.1049/2024/8929168.
26. Esmaeili-bandboni A, Amini SM, Faridi-majidi R, Bagheri J, Mohammadnejad J, Sadroddiny E. Cross-linking gold nanoparticles aggregation method based on localised surface plasmon resonance for quantitative detection of Mir-155. IET Nanobiotechnol. 2018;12(4):453–8. https://doi.org/10.1049/iet-nbt.2017.0174.
27. González-Ballesteros N, Rodríguez-Argüelles MC. Seaweeds: a promising bionanofactory for ecofriendly synthesis of gold and silver nanoparticles. In Sustainable Seaweed Technologies: Elsevier; 2020. p. 507–41.
28. Chaudhary R, Nawaz K, Khan AK, Hano C, Abbasi BH, Anjum S. An overview of the algae-mediated biosynthesis of nanoparticles and their biomedical applications. Biomolecules. 2020;10(11):1498.
29. Thiurunavukkarau R, Shanmugam S, Subramanian K, Pandi P, Muralitharan G, Arokiarajan M, Kasinathan K, Sivaraj A, Kalyanasundaram R, AlOmar SY, Shanmugam V. Silver nanoparticles synthesized from the seaweed *Sargassum polycystum* and screening for their biological potential. Sci Rep. 2022;12(1):14757.
30. Ody A, Thibaut T, Berline L, Changeux T, Andre JM, Chevalier C, Blanfune A, Blanchot J, Ruitton S, Stiger-Pouvreau V, Connan S. From In Situ to satellite observations of pelagic Sargassum distribution and aggregation in the Tropical North Atlantic Ocean. PLoS ONE. 2019;14(9):e0222584.
31. Rushdi MI, Abdel-Rahman IA, Saber H, Attia EZ, Abdelraheem WM, Madkour HA, Hassan HM, Elmaidomy AH, Abdelmohsen UR. Pharmacological and natural products diversity of the brown algae genus Sargassum. RSC Adv. 2020;10(42):24951–72.
32. Zhang R, Zhang X, Tang Y, Mao J. Composition, isolation, purification and biological activities of *Sargassum fusiforme* polysaccharides: a review. Carbohyd Polym. 2020;228:115381.
33. El-Sayed H, Abdelsalam A, Morad MY, Sonbol H, Ibrahim AM, Tawfik E. Phyto-synthesized silver nanoparticles from *Sargassum subrepandum*: anticancer, antimicrobial, and molluscicidal activities. Front Plant Sci. 2024;15:1403753.
34. Algotiml R, Gab-Alla A, Seoudi R, Abulreesh HH, El-Readi MZ, Elbanna K. Anticancer and antimicrobial activity of biosynthesized Red Sea marine algal silver nanoparticles. Sci Rep. 2022;12(1):2421.
35. Venkatesan J, Kim SK, Shim MS. Antimicrobial, antioxidant, and anticancer activities of biosynthesized silver nanoparticles using marine algae Ecklonia cava. Nanomaterials. 2016;6(12):235.
36. Bekele AZ, Gokulan K, Williams KM, Khare S. Dose and size-dependent antiviral effects of silver nanoparticles on feline calicivirus, a human norovirus surrogate. Foodborne Pathog Dis. 2016;13(5):239–44.
37. Wang ZX, Chen CY, Wang Y, Li FXZ, Huang J, Luo ZW, Rao SS, Tan YJ, Liu YW, Yin H, Wang YY. Ångstrom-scale silver particles as a promising agent for low-toxicity broad-spectrum potent anticancer therapy. Adv Func Mater. 2019;29(23):1808556.
38. Pei J, Fu B, Jiang L, Sun T. Biosynthesis, characterization, and anticancer effect of plant-mediated silver nanoparticles using *Coptis chinensis*. Int J Nanomed. 2019;14:1969–78.
39. Moussa Z, Ghoniem AA, Elsayed A, Alotaibi AS, Alenzi AM, Hamed SE, Elattar KM, Saber WI. Innovative binary sorption of Cobalt (II) and methylene blue by *Sargassum latifolium* using Taguchi and hybrid artificial neural network paradigms. Sci Rep. 2022;12(1):18291.
40. Ghoniem AA, Elattar KM, Alotaibi AS, Ghabban H, El Hersh MS, El-Khateeb AY, El-Amier YA, El-Gendy HM, Eldadamony NM, Saber WI, Elsayed A. Enhanced resistance of *Vigna unguiculata* to *Fusarium oxysporum* via *Rubia cordifolia* extract and growth-promoting endophytic Bacillus amyloliquefaciens DW6. Eur J Plant Pathol. 2024;170(3):567–91.
41. Ghoniem AA, Elattar KM, Al-Otibi FO, Elsayed A, El-Hersh MS, El-Khateeb AY, Helmy YA, Saber WI. Turmeric extract-mediated biogenic synthesis of Ag@SeO_2 magnetic nanoparticles: characterization, optimization, antibacterial and antioxidant activities. RSC Adv. 2024;14(10):7088–111.
42. Elattar KM, Ghoniem AA, Al-Askar AA, Bhgat El-Gazzar U, El-Hersh MS, Elsherbiny EA, Eldadamony NM, Saber WI. Melanin synthesized by the endophytic Aureobasidium Pullulans AKW: a multifaceted biomolecule with antioxidant, wound healing, and selective anticancer activity. Curr Topics Med Chem. 2024;24(24):2141–60.
43. Hammouda MM, Shalabi K, Alanazi AA, Elattar KM, Azzam MA, Rashed MM. Synthesis of novel benzopyrimido[4,5-*d*] azoninone analogs catalyzed by biosynthesized Ag-TiO_2 core/shell magnetic nanocatalyst and assessment of their antioxidant activity. RSC Adv. 2023;13(46):32532–46.
44. Hammouda MM, Alanazi AA, Elattar KM. *Mentha suaveolens* leaves extract-mediated synthesis of CoO@TiO_2 and Fe_2O_3@TiO_2 Core/Shell nanoparticles with synergistic antimicrobial and antioxidant activities. ChemistrySelect. 2024;9(17):e202401385.
45. Elattar KM, Ghoniem AA, Al-Otibi FO, El-Hersh MS, Helmy YA, Saber WI. Phytogenic synthesis and characterization of silver metallic/bimetallic nanoparticles using *Beta vulgaris* L. extract and assessments of their potential biological activities. Appl Sci. 2023;13(18):10110.
46. Leaves L, Leaves L. Antioxidant activity by DPPH radical scavenging method of ageratum conyzoides. Am J Ethnomed. 2014;1(4):244–9.
47. Boyanova L, Gergova G, Nikolov R, Derejian S, Lazarova E, Katsarov N, Krastev Z. Activity of Bulgarian propolis against 94 Helicobacter pylori strains *in vitro* by agar-well diffusion, agar dilution and disc diffusion methods. J Med Microbiol. 2005;54(5):481–3.
48. Veiga A, Maria da Graça TT, Rossa LS, Mengarda M, Stofella NC, Oliveira LJ, Murakami FS. Colorimetric microdilution assay: Validation of a standard method for determination of MIC, IC_{50}%, and IC_{90}% of antimicrobial compounds. J Microbiol Methods. 2019;162:50–61.

49. Al Balawi AN, Eldiasty JG, Mosallam SAER, El-Alosey AR, Elmetwalli A. Assessing multi-target antiviral and antioxidant activities of natural compounds against SARS-CoV-2: an integrated in vitro and in silico study. Bioresources and Bioprocessing. 2024;11(1):108.
50. Hassan MG, Farouk HS, Baraka DM, Khedr M, El Awady ME, Ameen F, Elmetwalli A. Pomegranate's silver bullet: Nature-powered nanoparticles deliver a one-two punch against cancer and antimicrobial resistance. Inorg Chem Commun. 2024;168:112853.
51. Elmetwalli A, Abdel-Monem MO, El-Far AH, Ghaith GS, Albalawi NAN, Hassan J, Hassan MG. Probiotic-derived silver nanoparticles target mTOR/MMP-9/BCL-2/dependent AMPK activation for hepatic cancer treatment. Med Oncol. 2024;41(5):106.
52. Elmetwalli A, El-Sewedy T, Hassan MG, Abdel-Monem MO, Hassan J, Ismail NF, El-Far AH. Gold nanoparticles mediate suppression of angiogenesis and breast cancer growth *via* MMP-9/NF-κB/mTOR and PD-L1/PD-1 signaling: integrative *in vitro* validation and network pharmacology insights. Naunyn Schmiedebergs Arch Pharmacol. 2024;398:7087–105. https://doi.org/10.1007/s00210-024-03682-8.
53. Ahmed SI, El-Sheekh MM, Akl FM, Makhlof ME, Abo-Neima SE. The brown seaweed *Sargassum latifolium* combined with low-level laser irradiation reduces hypercholesterolemia in rats by alleviating oxidative stress and inflammation. S Afr J Bot. 2024;172:686–700.
54. Abu Ahmed SE, Deyab MA, Hassan NI, El-Sheekh MM. Physicochemical characterization of *Sargassum latifolium* at Ras Sudr shores-red sea coast of Egypt. Egypt J Bot. 2022;62(3):763–76.
55. Olasehinde TA, Olaniran AO, Okoh AI. Macroalgae as a valuable source of naturally occurring bioactive compounds for the treatment of Alzheimer's disease. Mar Drugs. 2019;17(11):609.
56. Alavi M, Karimi N. Characterization, antibacterial, total antioxidant, scavenging, reducing power and ion chelating activities of green synthesized silver, copper and titanium dioxide nanoparticles using *Artemisia haussknechtii* leaf extract. Artif Cells Nanomed Biotechnol. 2018;46(8):2066–81.
57. Hosseinzadeh E, Foroumadi A, Firoozpour L. What is the role of phytochemical compounds as capping agents for the inhibition of aggregation in the green synthesis of metal oxide nanoparticles? A DFT molecular level response. Inorg Chem Commun. 2023;147:110243.
58. Amini SM. Preparation of antimicrobial metallic nanoparticles with bioactive compounds. Mater Sci Eng, C. 2019;103:109809.
59. Issaabadi Z, Nasrollahzadeh M, Sajadi SM. Efficient catalytic hydration of cyanamides in aqueous medium and in the presence of Naringin sulfuric acid or green synthesized silver nanoparticles by using *Gongronema latifolium* leaf extract. J Colloid Interface Sci. 2017;503:57–67.
60. Rani A, Saini KC, Bast F, Mehariya S, Bhatia SK, Lavecchia R, Zuorro A. Microorganisms: a potential source of bioactive molecules for antioxidant applications. Molecules. 2021;26(4):1142.
61. Bakhsh EM, Ismail M, Sharafat U, Akhtar K, Fagieh TM, Danish EY, Khan SB, Khan MI, Khan MA, Asiri AM. Highly efficient and recoverable Ag-Cu bimetallic supported catalyst applied for dyes and nitroarenes reduction. J Market Res. 2022;18:769–87. https://doi.org/10.1016/j.jmrt.2022.02.062.
62. Rayalu SS, Jose D, Joshi MV, Mangrulkar PA, Shrestha K, Klabunde K. Photocatalytic water splitting on Au/TiO2 nanocomposites synthesized through various routes: enhancement in photocatalytic activity due to SPR effect. Appl Catal B. 2013;142:684–93.
63. Mukherjee A, Sarkar D, Sasmal S. A review of green synthesis of metal nanoparticles using algae. Front Microbiol. 2021;12:693899.
64. Yulizar Y, Bakri R, Apriandanu DOB, Hidayat T. ZnO/CuO nanocomposite prepared in one-pot green synthesis using seed bark extract of *Theobroma cacao*. Nanostructures & Nano-Objects. 2018;16:300–5.
65. Seetharaman PK, Sivapunniyam A, Ramalingam P, Ramalingam KR, Liu B. Fabrication of a citrus flavonoid hesperetin-capped gold nanoparticles-reduced graphene oxide nanocomposites (Hes-Au/rGONCs) as a potential therapeutic agent for triple negative breast cancer and bacterial infections. Surfaces and Interfaces. 2023;42:103347.
66. Babu AT, Antony R. Green synthesis of silver doped nano metal oxides of zinc & copper for antibacterial properties, adsorption, catalytic hydrogenation & photodegradation of aromatics. J Environ Chem Eng. 2019;7(1):102840.
67. Cacua K, Ordoñez F, Zapata C, Herrera B, Pabón E, Buitrago-Sierra R. Surfactant concentration and pH effects on the zeta potential values of alumina nanofluids to inspect stability. Colloids Surf, A. 2019;583:123960.
68. Wang N, Hsu C, Zhu L, Tseng S, Hsu JP. Influence of metal oxide nanoparticles concentration on their zeta potential. J Colloid Interface Sci. 2013;407:22–8.
69. Odzak N, Kistler D, Behra R, Sigg L. Dissolution of metal and metal oxide nanoparticles in aqueous media. Environ Pollut. 2014;191:132–8.
70. Zhang J, Fan Y, Smith E. Experimental design for the optimization of lipid nanoparticles. J Pharm Sci. 2009;98(5):1813–9. https://doi.org/10.1002/jps.21549.
71. Thanh NT, Maclean N, Mahiddine S. Mechanisms of nucleation and growth of nanoparticles in solution. Chem Rev. 2014;114(15):7610–30.
72. Mozaffari S, Li W, Thompson C, Ivanov S, Seifert S, Lee B, Kovarik L, Karim AM. Colloidal nanoparticle size control: experimental and kinetic modeling investigation of the ligand–metal binding role in controlling the nucleation and growth kinetics. Nanoscale. 2017;9(36):13772–85.
73. Vorontsov AV, Tsybulya SV. Influence of nanoparticles size on XRD patterns for small monodisperse nanoparticles of Cu^0 and TiO_2 anatase. Ind Eng Chem Res. 2018;57(7):2526–36.
74. Patra JK, Baek KH. Green nanobiotechnology: factors affecting synthesis and characterization techniques. J Nanomater. 2014;2014(1):417305.
75. Zeng C, Liu C, Chen Y, Rosi NL, Jin R. Atomic structure of self-assembled monolayer of thiolates on a tetragonal Au92 nanocrystal. J Am Chem Soc. 2016;138(28):8710–3.
76. Sun Y, Gao S, Xie Y. Atomically-thick two-dimensional crystals: electronic structure regulation and energy device construction. Chem Soc Rev. 2014;43(2):530–46.
77. Mirkovic T, Ostroumov EE, Anna JM, Van Grondelle R, Govindjee, Scholes GD. Light absorption and energy transfer in the antenna complexes of photosynthetic organisms. Chem Rev. 2017;117(2):249–93.
78. McClements DJ. Advances in nanoparticle and microparticle delivery systems for increasing the dispersibility, stability, and bioactivity of phytochemicals. Biotechnol Adv. 2020;38:107287.
79. Elemike EE, Onwudiwe DC, Singh M. Eco-friendly synthesis of copper oxide, zinc oxide and copper oxide–zinc oxide nanocomposites, and their anticancer applications. J Inorg Organomet Polym Mater. 2020;30(2):400–9.
80. Fakhri A, Pourmand M, Khakpour R, Behrouz S. Structural, optical, photoluminescence and antibacterial properties of copper-doped silver sulfide nanoparticles. J Photochem Photobiol, B. 2015;149:78–83.
81. Endres SC, Ciacchi LC, Mädler L. A review of contact force models between nanoparticles in agglomerates, aggregates, and films. J Aerosol Sci. 2021;153:105719.

82. Sounart TL, Liu J, Voigt JA, Hsu JW, Spoerke ED, Tian ZHENG, Jiang YB. Sequential nucleation and growth of complex nanostructured films. Adv Func Mater. 2006;16(3):335–44.
83. Chamarthy SP, Pinal R. The nature of crystal disorder in milled pharmaceutical materials. Colloids Surf, A. 2008;331(1–2):68–75.
84. Lizundia E, Petisco S, Sarasua JR. Phase-structure and mechanical properties of isothermally melt-and cold-crystallized poly (L-lactide). J Mech Behav Biomed Mater. 2013;17:242–51.
85. Ashok CH, Rao KV, Chakra CS. Structural analysis of CuO nanomaterials prepared by novel microwave assisted method. J Atoms Mol. 2014;4(5):803–6.
86. Hashem AH, Abdel-Maksoud MA, Fatima S, Almutairi SM, Ghorab MA, El-Batal AI, El-Sayyad GS. Synthesis and characterization of innovative GA@ Ag-CuO nanocomposite with potent antimicrobial and anticancer properties. Sci Rep. 2025;15(1):689.
87. Farooq M, Shujah S, Tahir K, Hussain ST, Khan AU, Almarhoon ZM, Alabbosh KF, Alanazi AA, Althagafi TM, Zaki ME. Phytoassisted synthesis of CuO and Ag–CuO nanocomposite, characterization, chemical sensing of ammonia, degradation of methylene blue. Sci Rep. 2024;14(1):1618.
88. Abed Z, Mohammad RK, Elttayef A. Structural properties of Ag-CuO thin films on silicon prepared via DC magnetron sputtering. Egypt J Chem. 2022;65(4):685–91.
89. Phan MAT, Paterson J, Bucknall M, Arcot J. Interactions between phytochemicals from fruits and vegetables: effects on bioactivities and bioavailability. Crit Rev Food Sci Nutr. 2018;58(8):1310–29.
90. Achilonu MC, Umesiobi DO. Bioactive phytochemicals: bioactivity, sources, preparations, and/or modifications via silver tetrafluoroborate mediation. J Chem. 2015;2015(1):629085.
91. Alrefaee SH, Sefrji FO, Obaid R, Alsharari AM, Mojally M, Alisaac A, Alsahag M, El-Metwaly NM. Rosmarinus officinalis-based Ag/SiO_2 and CeO_2-Ag/SiO_2 core-shell nanocomposites: A green approach to phytochemical analyses, molecular docking, antioxidant and antimicrobial applications with enhanced biocompatibility. Results Eng. 2024;24:103478.
92. Hameed YA, Almahri A, Alalawy AI, Ibarhiam SF, Alkhathami ND, Mattar H, Alamoudi WM, El-Metwaly NM. Green synthesis and antimicrobial evaluation of Ag/TiO2 and Ag/SeO2 core-shell nanocomposites using r. Officinalis extract: a combined experimental and docking study. Inorg Chim Acta. 2025;574:122390.
93. Tsao R, Deng Z. Separation procedures for naturally occurring antioxidant phytochemicals. J Chromatogr B. 2004;812(1–2):85–99.
94. Shafey AME. Green synthesis of metal and metal oxide nanoparticles from plant leaf extracts and their applications: a review. Green Process Synth. 2020;9(1):304–39.
95. Young SL, Kellon JE, Hutchison JE. Small gold nanoparticles interfaced to electrodes through molecular linkers: a platform to enhance electron transfer and increase electrochemically active surface area. J Am Chem Soc. 2016;138(42):13975–84.
96. Ovais M, Khalil AT, Islam NU, Ahmad I, Ayaz M, Saravanan M, Shinwari ZK, Mukherjee S. Role of plant phytochemicals and microbial enzymes in biosynthesis of metallic nanoparticles. Appl Microbiol Biotechnol. 2018;102:6799–814.
97. Xie YY, Hu XH, Zhang YW, Wahid F, Chu LQ, Jia SR, Zhong C. Development and antibacterial activities of bacterial cellulose/graphene oxide-CuO nanocomposite films. Carbohyd Polym. 2020;229:115456.
98. Tavares TD, Antunes JC, Padrão J, Ribeiro AI, Zille A, Amorim MTP, Ferreira F, Felgueiras HP. Activity of specialized biomolecules against gram-positive and gram-negative bacteria. Antibiotics. 2020;9(6):314.
99. Santos RS, Figueiredo C, Azevedo NF, Braeckmans K, De Smedt SC. Nanomaterials and molecular transporters to overcome the bacterial envelope barrier: towards advanced delivery of antibiotics. Adv Drug Deliv Rev. 2018;136:28–48.
100. Díez-Pascual AM. Antibacterial action of nanoparticle loaded nanocomposites based on graphene and its derivatives: a mini-review. Int J Mol Sci. 2020;21(10):3563.
101. Kung ML, Tai MH, Lin PY, Wu DC, Wu WJ, Yeh BW, Hung HS, Kuo CH, Chen YW, Hsieh SL, Hsieh S. Silver decorated copper oxide (Ag@CuO) nanocomposite enhances ROS-mediated bacterial architecture collapse. Colloids Surf, B. 2017;155:399–407.
102. Zhu X, Wu D, Wang W, Tan F, Wong PK, Wang X, Qiu X, Qiao X. Highly effective antibacterial activity and synergistic effect of Ag-MgO nanocomposite against *Escherichia coli*. J Alloy Compd. 2016;684:282–90.
103. Navarre WW, Schneewind O. Surface proteins of gram-positive bacteria and mechanisms of their targeting to the cell wall envelope. Microbiol Mol Biol Rev. 1999;63(1):174–229.
104. Mei L, Lu Z, Zhang X, Li C, Jia Y. Polymer-Ag nanocomposites with enhanced antimicrobial activity against bacterial infection. ACS Appl Mater Interfaces. 2014;6(18):15813–21.
105. Tambosi R, Liotenberg S, Bourbon ML, Steunou AS, Babot M, Durand A, Kebaili N, Ouchane S. Silver and copper acute effects on membrane proteins and impact on photosynthetic and respiratory complexes in bacteria. MBio. 2018;9(6):10–1128.
106. Khina AG, Krutyakov YA. Similarities and differences in the mechanism of antibacterial action of silver ions and nanoparticles. Appl Biochem Microbiol. 2021;57:683–93.
107. Mostafa, M., Almoammar, H. and Abd-Elsalam, K.A., 2018. Nanoantimicrobials mechanism of action. *Nanobiotechnology Applications in Plant Protection*, pp.281–322.
108. Khorsandi K, Hosseinzadeh R, Sadat Esfahani H, Keyvani-Ghamsari S, Ur Rahman S. Nanomaterials as drug delivery systems with antibacterial properties: current trends and future priorities. Expert Rev Anti Infect Ther. 2021;19(10):1299–323.
109. Elbasuney S, Yehia M, Ismael S, Al-Hazmi NE, El-Sayyad GS, Tantawy H. Potential impact of reduced graphene oxide incorporated metal oxide nanocomposites as antimicrobial, and antibiofilm agents against pathogenic microbes: bacterial protein leakage reaction mechanism. J Cluster Sci. 2023;34(2):823–40.
110. Mammari N, Lamouroux E, Boudier A, Duval RE. Current knowledge on the oxidative-stress-mediated antimicrobial properties of metal-based nanoparticles. Microorganisms. 2022;10(2):437.
111. Tauran Y, Brioude A, Coleman AW, Rhimi M, Kim B. Molecular recognition by gold, silver, and copper nanoparticles. World J Biol Chem. 2013;4(3):35.
112. Flores-López LZ, Espinoza-Gómez H, Somanathan R. Silver nanoparticles: Electron transfer, reactive oxygen species, oxidative stress, beneficial and toxicological effects. Mini review. J Appl Toxicol. 2019;39(1):16–26.
113. Volpe CMO, Villar-Delfino PH, Dos Anjos PMF, Nogueira-Machado JA. Cellular death, reactive oxygen species (ROS) and diabetic complications. Cell Death Dis. 2018;9(2):119.
114. Mei L, Lu Z, Zhang W, Wu Z, Zhang X, Wang Y, Luo Y, Li C, Jia Y. Bioconjugated nanoparticles for attachment and penetration into pathogenic bacteria. Biomaterials. 2013;34(38):10328–37.
115. Mejia-Mendez JL, Reza-Zaldívar EE, Sanchez-Martinez A, et al. Exploring the cytotoxic and antioxidant properties of lanthanide-doped ZnO nanoparticles: a study with machine learning interpretation. J Nanobiotechnol. 2024;22:687. https://doi.org/10.1186/s12951-024-02957-9.
116. Javed R, Sajjad A, Naz S, Sajjad H, Ao Q. Significance of capping agents of colloidal nanoparticles from the perspective of drug and gene delivery, bioimaging, and biosensing: an insight. Int J Mol Sci. 2022;23(18):10521.

117. Fierascu I, Fierascu IC, Brazdis RI, Baroi AM, Fistos T, Fierascu RC. Phytosynthesized metallic nanoparticles, between nanomedicine and toxicology. A brief review of 2019′ s findings. Materials. 2020;13(3):574.
118. Behzadi S, Serpooshan V, Tao W, Hamaly MA, Alkawareek MY, Dreaden EC, Mahmoudi M. Cellular uptake of nanoparticles: journey inside the cell. Chem Soc Rev. 2017;46(14):4218–44.
119. Woźniak-Budych MJ, Staszak K, Staszak M. Copper and copper-based nanoparticles in medicine—perspectives and challenges. Molecules. 2023;28(18):6687.
120. El-Zayat MM, Eraqi MM, Alrefai H, El-Khateeb AY, Ibrahim MA, Aljohani HM, Elshaer MM. The antimicrobial, antioxidant, and anticancer activity of greenly synthesized selenium and zinc composite nanoparticles using *Ephedra aphylla* extract. Biomolecules. 2021;11(3):470.
121. Xue Y, Zhang T, Zhang B, Gong F, Huang Y, Tang M. Cytotoxicity and apoptosis induced by silver nanoparticles in human liver HepG2 cells in different dispersion media. J Appl Toxicol. 2016;36(3):352–60.
122. Harwansh RK, Deshmukh R, Shukla VP, Khunt D, Prajapati BG, Rashid S, Ali N, Elossaily GM, Suryawanshi VK, Kumar A. Recent advancements in gallic acid-based drug delivery: applications, clinical trials, and future directions. Pharmaceutics. 2024;16(9):1202.
123. Raja G, Jang YK, Suh JS, Kim HS, Ahn SH, Kim TJ. Microcellular environmental regulation of silver nanoparticles in cancer therapy: a critical review. Cancers. 2020;12(3):664.
124. Shi Y, Wu Z, Qi M, Liu C, Dong W, Sun W, Bai X. Multiscale bioresponses of metal nanoclusters. Adv Mater. 2024;36(13):2310529.
125. Hamida RS, Albasher G, Bin-Meferij MM. Oxidative stress and apoptotic responses elicited by nostoc-synthesized silver nanoparticles against different cancer cell lines. Cancers. 2020;12(8):2099.
126. Felix LP, Perez JE, Contreras MF, Ravasi T, Kosel J. Cytotoxic effects of nickel nanowires in human fibroblasts. Toxicol Rep. 2016;3:373–80.

Authors and Affiliations

Khaled M. Elattar[1] · Alaa Elmetwalli[2] · Othman R. Alzahrani[3] · Abeer A. Ghoniem[4] · Mervat G. Hassan[5] · Sara Abdelsayed[5] · Ahmed A. Zaher[6] · Deema Kamal Sabir[7] · Ashraf Elsayed[8]

✉ Alaa Elmetwalli
aelmetealli@ut.edu.sa; dr.prof2011@gmail.com

[1] Unit of Genetic Engineering and Biotechnology, Mansoura University, El-Gomhoria St., Mansoura 35516, Egypt

[2] Prince Fahad bin Sultan Research Chair for Biomedical Research, University of Tabuk, Tabuk, Saudi Arabia 47713

[3] Department of Biology, Faculty of Science, University of Tabuk, Tabuk 47512, Saudi Arabia

[4] Microbial Activity Unit, Department of Microbiology, Soils, Water and Environment Research Institute, Agricultural Research Center, Giza 12619, Egypt

[5] Department of Botany and Microbiology, Faculty of Science, Benha University, Benha 33516, Egypt

[6] Chemistry Department, Faculty of Science, Mansoura University, Mansoura 35516, Egypt

[7] Department of Medical Surgical Nursing, College of Nursing, Princess Nourah bint Abdulrahman University, P.O.Box 84428, Riyadh 11671, Saudi Arabia

[8] Botany Department, Faculty of Science, Mansoura University, Mansoura 35516, Egypt